Effect of the Precipitation of Neutral-Soap, Acid-Soap, and Alkanoic Acid Crystallites on the Bulk pH and Surface Tension of Soap Solutions

Peter A. Kralchevsky,*,† Krassimir D. Danov,† Cenka I. Pishmanova,† Stefka D. Kralchevska,† Nikolay C. Christov,† Kavssery P. Ananthapadmanabhan,‡ and Alex Lips‡

Laboratory of Chemical Physics & Engineering, Faculty of Chemistry, University of Sofia, 1164 Sofia, Bulgaria, and Unilever Research & Development, Trumbull, Connecticut 06611

Received August 30, 2006. In Final Form: January 4, 2007

The natural pH of sodium dodecanoate (laurate), NaL, and sodium tetradecanoate (myristate), NaMy, solutions is measured as a function of the surfactant concentrations at 25 °C, and at several fixed NaCl concentrations. Surface tension isotherms are also obtained. Depending on the surfactant concentration, the investigated solutions contain precipitates of alkanoic acid, neutral soap, and acid soaps. The latter are complexes of alkanoic acid and neutral soap with a definite stoichiometry. A method for identification of the different precipitates from the experimental pH isotherms is developed. It is based on the analysis of precipitation diagrams, which represent plots of characteristic functions. This analysis reveals that for the NaL solutions there are three concentration regions with different precipitates, including lauric acid and 1:1 acid soap. In the case of NaMy solutions, we identified the existence of concentration regions with precipitates of myristic acid: 4:1, 3:2, and 1:1 acid soaps, and coexistence of two solid phases: 1:1 acid soap and neutral soap. The solubility products of the precipitates have been determined. Modeling the acid soaps of different stoichiometry as solid solutions of alkanoic acid and 1:1 acid soap, we derived a theoretical expression for their solubility products, which agrees well with the experiment. The kinks in the surface-tension isotherms of the investigated solutions correspond to some of the boundaries between the regions with different precipitates in the bulk. The theoretical analysis indicates that for the NaL solutions the adsorption layer is composed mostly of lauric acid, while for the NaMy solutions + 10 mM NaOH the adsorption layer is composed of nondissociated molecules of neutral soap. The developed approach could be applied to analyze the type of precipitates and the behavior of the surface tension for solutions of sodium and potassium alkanoates with different chain lengths at various temperatures and concentrations.

1. Introduction

The sodium and potassium alkanoates (laurates, myristates, palmitates, stearates, etc.) have attracted both academic and industrial interest because of their application in many consumer products: soap bars; cleaning products; cosmetics; facial cleaners; shaving creams; deodorants; and topical-delivered products.[1−3] The dissolution of such alkanoates (carboxylates) in water is accompanied by increase of pH, which is due to protonation (hydrolysis) of the alkanoate anion:[4]

$$Z^- + H_2O \leftrightarrow HZ + OH^- \qquad (1.1)$$

Here and hereafter we use the notations in ref 4, viz., Z^- is alkanoate (laurate, myristate, palmitate, ...) anion, whereas HZ is nondissociated alkanoic (fatty) acid. The alkanoic acids with 12 and more carbon atoms are weakly soluble in water. So, their production in the reaction, eq 1.1, leads to the precipitation of HZ microcrystallites, which cause the typical turbidity of the soap solutions. Moreover, the hydrogen-bonding interaction between the alkanoic acid molecules and alkanoate ions leads to the formation of acid-soap complexes and crystallites:[5−9]

$$HZ + Z^- + M^+ \leftrightarrow MHZ_2 \leftrightarrow \text{precipitates} \qquad (1.2)$$

Here, M^+ is a metal cation (usually Na^+ or K^+), and MHZ_2 is acid soap. The first detailed studies on acid soaps were published by Ekwall et al.[5−7,10−12] and McBain et al.[8,9] Since then, many other results on acid soaps have been reported.[3,4,13−20]

* Corresponding author. Phone: (+359) 2-962 5310. Fax: (+359) 2-962 5438. E-mail: pk@lcpe.uni-sofia.bg.

† University of Sofia.

‡ Unilever Research & Development.

(1) Porter, M. R. *Handbook of Surfactants*; Blackie Academic & Professional: London, 1997; p 100.

(2) Bartolo R. G.; Lynch M. L. *Kirk-Othmers Encyclopedia of Chemical Technologies*, 4th ed.; Wiley: New York, 1997.

(3) Lynch, M. L.; Wireko, F.; Tarek, M.; Klein, M. Intermolecular interactions and the structure of fatty acid−soap crystals. *J. Phys. Chem. B* **2001**, *105*, 552−561.

(4) Lucassen, J. Hydrolysis and precipitates in carboxylate soap solutions. *J. Phys. Chem.* **1966**, *70*, 1824−1830.

(5) Ekwall, P.; Mylius, W. Über saure Natriumsalze der Palmitinsäure. *Ber. Dtsch. Chem. Ges.* **1929**, *62*, 1080−1084.

(6) Ekwall, P.; Mylius, W. Über saure Natriumsalze der Laurinsäure. *Ber. Dtsch. Chem. Ges.* **1929**, *62*, 2687−2690.

(7) Ekwall, P. Das System Palmitinsäure-Natriumpalmitat. *Z. Anorg. Allg. Chem.* **1933**, *210*, 337−349.

(8) McBain, J. W.; Field, M. C. Phase rule equilibria of acid soaps. I. Anhydrous acid potassium laurate. *J. Phys. Chem.* **1933**, *37*, 675−684.

(9) McBain, J. W.; Field, M. C. Phase rule equilibria of acid soaps. II. Anhydrous acid sodium palmitates. *J. Chem. Soc.* **1933**, 920−924.

(10) Ekwall, P. Zur Kenntnis der Konstitution der verdünnten Seifenlösungen. III. Die Theorie der Hydrolyse. *Kolloid-Z.* **1940**, *92*, 141−157.

(11) Ekwall, P.; Lindblad, L. G. Zur Kenntnis der Konstitution der verdünnten Seifenlösungen. IV. Die Hydroxylionenaktivität der Natriumlauratlösungen bei 20 °C. *Kolloid-Z.* **1941**, *94*, 42−57.

(12) Ekwall, P. Solutions of alkali soaps and water in fatty acids. *Colloid Polym. Sci.* **1988**, *266*, 279−282.

(13) Lynch, M. L.; Pan, Y.; Laughlin, R. G. Spectroscopic and thermal characterization of 1:2 sodium soap/fatty acid acid−soap crystals. *J. Phys. Chem.* **1996**, *100*, 357−361.

(14) Lynch, M. L. Acid−soaps. *Curr. Opin. Colloid Interface Sci.* **1997**, *2*, 495−500.

(15) Wen, X.; Franses, E. I. Effect of protonation on the solution and phase behavior of aqueous sodium myristate. *J. Colloid Interface Sci.* **2000**, *231*, 42−51.

10.1021/la0625401 CCC: $37.00
Published on Web 02/24/2007

The quantitative theory of alkanoate (carboxylate) soap solutions was developed by Lucassen.[4] It describes the equilibrium composition of the solutions and their pH, which is in good agreement with experimental data for potassium carboxylates. The presence of anionic (Z^-) and nonionic (HZ) amphiphiles in such solutions leads to a complicated concentration dependence of their surface tension.[21,22] Despite the presence of crystalline precipitates, the sodium alkanoates are known to reduce significantly the surface tension. For example, at room temperature the sodium myristate can reduce the surface tension of water from 72 to 10 mN/m.[21] The complex behavior of the surface tension of such solutions could be related to the fact that the alkanoic acids and alcohols of longer paraffin chains exhibit surface phase transitions.[23−27] In addition, the adsorbed fatty acid molecules could form complexes with the alkanoate anions,[12] and with other surfactants and polyelectrolytes.[28,29] The plots of experimental data for the electroconductivity, or surface tension, vs the total input concentration of sodium alkanoate exhibit one or several kinks, which have been attributed to critical micelle concentrations (CMC).[30] The situation seems simpler only in the case of high pH (obtained by addition of NaOH), where alkanoic acid and precipitates are missing, and the solute could be treated as a simple anionic surfactant (Z^-).[31−34]

The solubility boundaries (Kraft points) of long-chain sodium alkanoates have been examined,[35] and the effects of simple inorganic salts and bulky organic cations on alkanoate solubility have been investigated.[36] Ca^{2+} ions were found to enhance the precipitation. The contact angles of precipitates in sodium and calcium alkanoate solutions were studied in relation to their defoaming action.[37−40]

In the present article, we combine experiment and theory to investigate the type of crystallites formed in aqueous solutions of sodium dodecanoate (laurate), NaL, and sodium tetradecanoate (myristate), NaMy, at room temperature (25 °C), in the presence or absence of added NaCl. The type of crystalline precipitates depends on the concentration and composition of the investigated solutions. At the lowest concentrations, precipitates are missing.[4] With the rise of the alkanoate concentration, one could observe the formation of precipitates of alkanoic acid, acid soap, and coexistence of two-phase precipitates, e.g., acid soap and neutral soap.[4]

In general, the formula of the acid soap is $H_jM_nZ_{j+n}$. It could be considered as being composed of j molecules of alkanoic acid (HZ) and n molecules of neutral soap (MZ). It is often termed j:n acid soap: $(HZ)_j(MZ)_n$. Acid soaps of different stoichiometry, j:n = 1:1, 1:2, 2:1, 3:2, 4:1, etc., have been experimentally detected.[3,12−14,19,20]

Our first goal in the present paper is by analysis of pH isotherms to determine the composition of the NaL and NaMy solutions at various concentrations and to identify the type of precipitates: alkanoic acid (HZ), j:n acid soaps ($H_jM_nZ_{j+n}$), neutral soap (MZ), and two-phase precipitates. In particular, we will determine the solubility constants (products) for all observed precipitates and will interpret their values in terms of the theory of solid solutions, applied to acid soaps. Our second goal is to interpret the surface tension isotherms of NaL and NaMy based on the information about the composition of the bulk solution obtained from the analysis of the pH data. This is a nontrivial task because, as already mentioned, the formation of different precipitates affects the bulk concentrations of the amphiphilic species.

The article is organized as follows. In section 2, the experimental procedures are described and the obtained results are presented. In section 3, theoretical expressions for pH and concentrations of the various species are derived for the cases when different precipitates are present. Section 4 describes the method of precipitate characteristic functions, which enables one to establish the type of precipitates that are present in the investigated solutions. The theoretical analysis of the experimental data for the pH and surface tension NaL and NaMy, respectively, is presented in sections 5 and 6. Theoretical interpretation of the experimentally determined solubility products of acid soaps is given in section 7. Finally, in section 8 we interpret the experimental surface tension isotherms of NaMy in the presence of 10 mM NaOH.

2. Experimental Section

2.1. Materials and Experimental Procedures. In our experiments, sodium laurate, NaL, and sodium myristate, NaMy, >99%

(16) Wen, X.; Lauterbach, J.; Franses, E. I. Surface densities of adsorbed layers of aqueous sodium myristate inferred from surface tension and infrared reflection absorption spectroscopy. *Langmuir* **2000**, *16*, 6987−6994.
(17) Kanicky, J. R.; Shah, D. O. Effect of premicellar aggregation on the p*K*a of fatty acid soap solutions. *Langmuir* **2003**, *19*, 2034−2038.
(18) Saitta, A. M.; Klein, M. L. Proton tunneling in fatty acid/soap crystals? *J. Chem. Phys.* **2003**, *118*, 1−3.
(19) Heppenstall-Butler, M.; Butler, M. F. Nonequilibrium behavior in the three-component system stearic acid−sodium stearate−water. *Langmuir* **2003**, *19*, 10061−10072.
(20) Zhu, S.; Heppenstall-Butler, M.; Butler, M. F.; Pudney, P. D. A.; Ferdinando, D.; Mutch, K. J. Acid soap and phase behavior of stearic acid and triethanolamine stearate. *J. Phys. Chem. B.* **2005**, *109*, 11753−11761.
(21) Wen, X.; McGinnis, K. C.; Franses, E. I. Unusually low dynamic surface tension of aqueous solutions of sodium myristate. *Colloids Surf. A.* **1998**, *143*, 371−380.
(22) Coltharp, K. A.; Franses, E. I. Equilibrium and dynamic surface tension behavior of aqueous soaps: sodium octanoate and sodium dodecanoate (sodium laurate). *Colloids Surf. A.* **1996**, *108*, 225−242.
(23) Kaganer, V. M.; Möhwald, H.; Dutta, P. Structure and phase transitions in Langmuir monolayers. *Rev. Mod. Phys.* **1999**, *71*, 779−819.
(24) Petrov, J. G.; Pfohl, T.; Möhwald, H. Ellipsometric chain length dependence of fatty acid Langmuir monolayers. A heads-and-tails model. *J. Phys. Chem. B* **1999**, *103*, 3417−3424.
(25) Ferri, J. K.; Stebe, K. J. Soluble surfactants undergoing surface phase transitions. *J. Colloid Interface Sci.* **1999**, *209*, 1−9.
(26) Casson, B. D.; Bain, C. D. Unequivocal evidence for a liquid−gas phase transition in monolayers of decanol adsorbed at the air/water interface. *J. Am. Chem. Soc.* **1999**, *121*, 2615−2616.
(27) Danov, K. D.; Kralchevsky, P. A.; Ananthapadmanabhan, K. P.; Lips, A. Interpretation of surface-tension isotherms of n-alkanoic (fatty) acids by means of the van der Waals model. *J. Colloid Interface Sci.* **2006**, *300*, 809−813.
(28) Hand, S.; Yang, J. Self-assembly of lamellar structures of fatty acids complexed with surfactant in aqueous solutions. *Langmuir* **1998**, *14*, 3597−3601.
(29) Gole, A.; Phadtare, S.; Sastry, M.; Langevin, D. Studies on interaction between similarly charged polyelectrolyte: fatty acid system. *Langmuir* **2003**, 9321−9327.
(30) Zimmels, Y.; Lin, I. Y. Stepwise association properties of some surfactant aqueous solutions. *Colloid Polym. Sci.* **1974**, *252*, 594−612.
(31) Lucassen-Reynders, E. H. A surface equation of state for mixed surfactant monolayers. *J. Colloid Interface Sci.* **1972**, *41*, 156−167.
(32) van den Bogaert, R.; Joos, P. Diffusion-controlled adsorption kinetics for a mixture of surface active agents at the solution-air interface. *J. Phys. Chem.* **1980**, *84*, 190−194.
(33) Zwierzykowski, W.; Konopacka-Lyskawa, D. Estimation of dielectric constants of adsorbed monolayers for some sodium soap solutions. *J. Colloid Interface Sci.* **1999**, *218*, 265−268.
(34) Fainerman, V. B.; Miller, R.; Möhwald, H. General relationships of the adsorption behavior of surfactants at the water/air interface. *J. Phys. Chem. B* **2002**, *106*, 809−819.
(35) de Mul, M. N. G.; Davis, T. D.; Evans, D. F.; Bhave, A. V.; Wagner, J. R. Solution phase behavior and solid phase structure of long-chain sodium soap mixtures. *Langmuir* **2000**, *16*, 8276−8284.
(36) Lin, B.; McCormick, A. V.; Davis, H. T.; Strey, R. Solubility of sodium soaps in aqueous salt solutions. *J. Colloid Interface Sci.* **2005**, *291*, 543−549.
(37) Luangpirom, N.; Dechabumphen, N.; Saiwan, C.; Scamehorn, J. F. Contact angle of surfactant solutions on precipitated surfactant surfaces. *J. Surfactants Deterg.* **2001**, *4*, 367−373.
(38) Ballasuwatthi, P.; Dechabumphen, N.; Saiwan, C.; Scamehorn, J. F. Contact angle of surfactant solutions on precipitated surfactant surfaces. II. Effects of surfactant structure, presence of a subsaturated surfactant, pH, and counterion/surfactant ratio. *J. Surfactants Deterg.* **2004**, *7*, 31−40.
(39) Luepakdeesakoon, B.; Saiwan, C.; Scamehorn, J. F. Contact angle of surfactant solutions on precipitated surfactant surfaces. III. Effects of subsaturated anionic and nonionic surfactants and NaCl. *J. Surfactants Deterg.* **2006**, *9*, 125−136.
(40) Zhang, H.; Miller, C. A.; Garrett, P. R.; Raney, K. H. Mechanism for defoaming by oils and calcium soap in aqueous systems. *J. Colloid Interface Sci.* **2003**, *263*, 633−644.

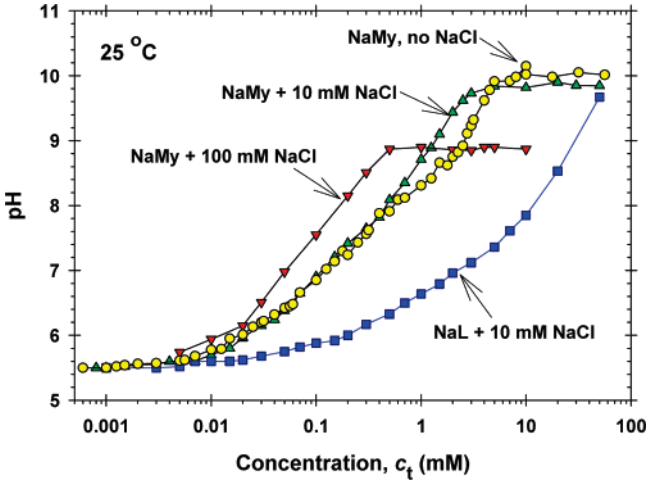

Figure 1. Experimental dependence of the pH of solutions of sodium soaps (NaL and NaMy) on the total input soap concentration, c_t, at fixed concentrations of NaCl denoted in the figure.

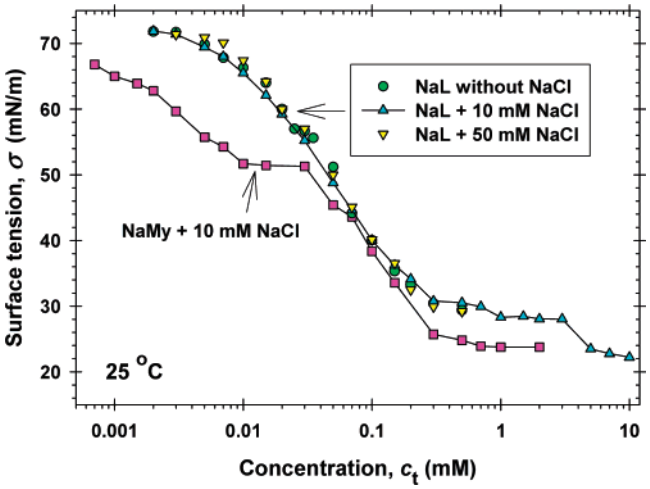

Figure 2. Experimental dependence of the surface tension, σ, of solutions of sodium soaps (NaL and NaMy) on the total input soap concentration, c_t, at fixed concentrations of NaCl denoted in the figure.

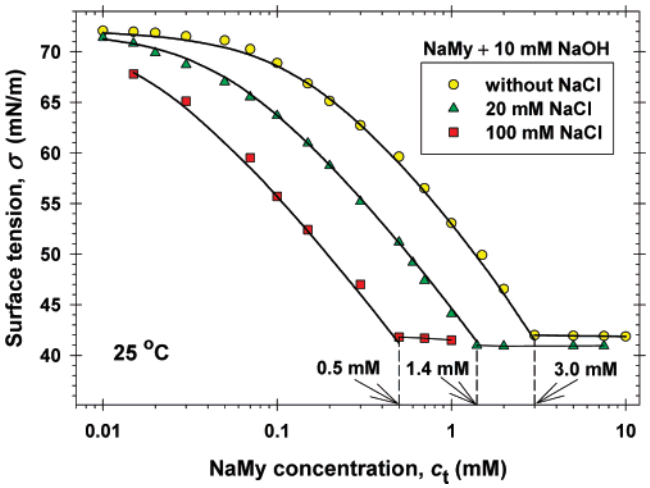

Figure 3. Experimental surface tension isotherms, σ vs c_t, for NaMy solutions containing 10 mM NaOH. The three curves correspond to three different fixed concentrations of NaCl denoted in the figure.

pure (product of TCI, Tokyo, Japan), and NaCl (product of Merck) were used. The solutions were prepared by water that had been initially deionized (Milli Q 185 plus, Millipore, USA), and then equilibrated with the atmospheric CO_2, so its pH was 5.5. The NaL and NaMy were completely dissolved in water by heating the solutions to 45 and 60 °C, respectively, and stirring for 30 min. Thus a concentrated stock solution was obtained, from which the working solutions were prepared by dilution. Next, the solutions were cooled down to 25 °C and kept at this temperature for 24 h in a closed vessel to attain equilibrium between the solution and the precipitating crystallites. Finally, we carried out measurements of the solutions' pH and surface tension, σ. The latter was measured by means of the Wilhelmy-plate method (tensiometer Krüss 10ST), and pendent drop method (Drop Shape Analysis System DSA 10, Krüss GmbH, Hamburg).

Visually, at the same concentration the solutions of NaMy contain more precipitates than those of NaL. At concentrations above 5 mM and 25 °C, the solutions of NaMy resemble a jelly. The respective pH values were measured in this jelly after stirring.

For the solutions without added NaOH, the kinetics of relaxation of the surface tension, σ, is relatively slow. After a sufficiently long period of time (10−30 min) the time dependence of surface tension reaches a plateau. The value of σ at this plateau was taken as equilibrium surface tension. The obtained values of σ are not very well reproducible. To overcome this difficulty, each experimental point for σ is obtained by averaging of the results of at least five separate measurements by the two methods (Wilhelmy plate and pendent drop).

In contrast, the relaxation of σ is very fast for the NaMy solutions containing 10 mM NaOH: the equilibrium is attained within 3 s, and the results for σ are well reproducible. At the highest investigated concentrations, precipitates appear also in the solutions with 10 mM NaOH.

2.2. Experimental Results. The points in Figure 1 show the experimental dependence of pH on the total input concentration, c_t, of NaL or NaMy. The solutions of NaL contained 10 mM added NaCl. The three curves for NaMy contained 0, 10, and 100 mM added NaCl. As seen in Figure 1, the pH of the solutions with NaMy is systematically greater than the pH of the NaL solution, at the same c_t. At the greatest c_t, the pH isotherms of the solutions of NaMy exhibit a plateau, whose level decreases with the increase of the NaCl concentration. Moreover, the addition of NaCl leads to a shift of the pH isotherms leftward. Theoretical interpretation of the experimental curves in Figure 1 is given in sections 5 and 6.

Figure 2 shows experimental surface tension isotherms for NaMy with 10 mM NaCl, and for NaL with 0, 10, and 50 mM NaCl. The results show that the effect of NaCl on the surface tension isotherm of NaL is negligible. Both the isotherms with NaL and NaMy exhibit kinks, whose nature will be discussed in sections 5.3, 6.2, and 8.1.

Figure 3 presents experimental surface-tension isotherms of NaMy solutions containing 10 mM NaOH. The three curves correspond to three different fixed concentrations of NaCl: 0, 20, and 100 mM. In this case, the addition of NaCl leads to a decrease in the surface tension. Each of the three experimental curves exhibits a kink and plateau at the highest concentrations. At concentrations lower than that of the kink, the solutions are transparent. At concentrations greater than that of the kink, formation of precipitates is observed. Interpretation of the surface tension isotherms of NaMy + 10 mM NaOH is given in section 8.

3. Theoretical Section

3.1. Basic Equations. Here, we present the theory of the pH of aqueous solutions of alkali metal carboxylates, such as sodium and potassium laurates, myristates, palmitates, etc. As a basis, we will use the theory of the pH of carboxylate soap solutions developed by Lucassen,[4] which will be upgraded to account for the presence of dissolved NaCl, NaOH, and CO_2. The theory of such solutions is nontrivial because of the possible existence of several concentration regions with different precipitates: (i) no precipitate; (ii) precipitate of alkanoic acid; (iii) precipitates of j:n acid soaps (j,n = 1, 2, 3, ...); (iv) precipitate of neutral soap; (v) coexistence of acid and neutral soap; (vi) appearance of micelles, etc. As mentioned above, we will denote by Z^- the

alkanoate (laurate, myristate, ...) anion; by M^+, metal cation (usually Na^+ or K^+); by HZ, alkanoic (fatty) acid; by MZ, neutral soap; by $(HZ)_j(MH)_n$, acid soap of composition HZ:MZ = *j*:*n*; by A^-, anion due to the added salt, MA. (In our experiments, MA = NaCl, and $A^- = Cl^-$.)

Three of the basic equations express the dissociation equilibria of the fatty acid (HZ) and neutral soap (MZ) molecules, and the electroneutrality of the solution:

$$c_H c_Z \gamma_\pm^2 = K_A c_{HZ} \tag{3.1}$$

$$c_M c_Z \gamma_\pm^2 = Q_{MZ} c_{MZ} \tag{3.2}$$

$$c_M + c_H = c_{OH} + c_{HCO_3} + c_Z + c_A \tag{3.3}$$

c is the concentration of the component denoted by the respective subscript; K_A and Q_{MZ} are the dissociation constants of HZ and MZ, respectively. In the literature, we find values $K_A = 1.25 \times 10^{-5}$ (ref 4) and $K_A = 1.995 \times 10^{-5}$ (ref 41). Here and hereafter, the concentrations in the equilibrium constants are expressed in molarity (M). Q_{MZ} will be determined in section 8. $\gamma_\pm$ is the activity coefficient, which can be calculated from the known semiempirical formula,[42]

$$\log \gamma_\pm = -\frac{A\sqrt{I}}{1 + Bd_i\sqrt{I}} + bI \tag{3.4}$$

originating from the Debye−Hückel theory; I (M) is the ionic strength of the solution; d_i is the diameter of the ion; A, B, and b are parameters which are tabulated in the book by Robinson and Stokes;[42] for our experimental conditions, we used the values $A = 0.5115\ M^{-1/2}$, $Bd_i = 1.316\ M^{-1/2}$, and $b = 0.055\ M^{-1}$. In the considered case, the ionic strength can be estimated from the expression $I \approx c_A + c_B + c_t$, where c_A, c_B, and c_t stand, respectively, for the input concentrations of inorganic salt (NaCl), base (NaOH), and total concentration of carboxylate.

In the right-hand side of the electroneutrality condition, eq 3.3, we have taken into account the presence of hydroxyl, OH^-, and hydrocarbonate, HCO_3^-. From the equilibrium of the reactions $H^+ + OH^- \leftrightarrow H_2O$ and $H^+ + HCO_3^- \leftrightarrow CO_2 + H_2O$, we obtain

$$c_H c_{OH} \gamma_\pm^2 = K_W = 6.81 \times 10^{-15} \tag{3.5}$$

$$c_H c_{HCO_3} \gamma_\pm^2 = k_{CO_2} S_{CO_2} \equiv K_{CO_2} \tag{3.6}$$

Here, K_W is the dissociation constant of water; k_{CO_2} is an equilibrium constant; S_{CO_2} is the concentration of dissolved CO_2; K_{CO_2} is defined by eq 3.6. At temperature 25 °C, the experiment gives $pH \equiv -\log(c_H\gamma_\pm) \approx 5.5$ for pure water equilibrated with the atmospheric air. Then, from eq 3.6 (with $c_{HCO_3} = c_H$ and $\gamma_\pm \approx 1$) one estimates $K_{CO_2} \approx 1 \times 10^{-11}$. Substituting c_{OH} and c_{HCO3} from eqs 3.5 and 3.6 into the electroneutrality condition, eq 3.3, we obtain

$$c_M + c_H = \frac{K_H}{c_H \gamma_\pm^2} + c_Z + c_A \tag{3.7}$$

$$K_H \equiv K_W + K_{CO_2} \tag{3.8}$$

The amounts of the components M and Z incorporated in the solid phase (in the crystallites) per unit volume are given by the equations[4]

$$m_M = c_t + c_A + c_B - c_M - c_{MZ} \tag{3.9}$$

$$m_Z = c_t - c_Z - c_{HZ} - c_{MZ} \tag{3.10}$$

As before, c_{HZ} and c_{MZ} are the concentrations of dissolved (but nondissociated) HZ and MZ molecules.

3.2. Solutions without Precipitates. In this case, $m_M = m_Z = 0$, and from eqs 3.9 and 3.10 we obtain

$$c_t + c_A + c_B = c_M + c_{MZ} \tag{3.11}$$

$$c_t = c_Z + c_{HZ} + c_{MZ} \tag{3.12}$$

From eqs 3.1 and 3.12 we can express c_Z and c_{HZ}:

$$c_Z = \frac{\tilde{K}_A(c_t - c_{MZ})}{\tilde{K}_A + c_H} \approx \frac{\tilde{K}_A c_t}{\tilde{K}_A + c_H} \tag{3.13}$$

$$c_{HZ} = \frac{c_H(c_t - c_{MZ})}{\tilde{K}_A + c_H} \approx \frac{c_H c_t}{\tilde{K}_A + c_H} \tag{3.14}$$

where $\tilde{K}_A \equiv K_A/\gamma_\pm^2$; at the last step we have used the fact that usually $c_{MZ} \ll c_t$. To determine c_{MZ}, in eq 3.2 we substitute c_M from eq 3.11 and c_Z from eq 3.13. Neglecting the quadratic term with respect to c_{MZ}, we obtain

$$c_{MZ} \approx \frac{(c_A + c_B + c_t)c_t}{(1 + c_H/\tilde{K}_A)\tilde{Q}_{MZ} + c_A + c_B + 2c_t} \tag{3.15}$$

where $\tilde{Q}_{MZ} \equiv Q_{MZ}/\gamma_\pm^2$.

Finally, in the electroneutrality equation, eq 3.7, we substitute c_M from eq 3.11 and c_Z from eq 3.13. After some transformations, we derive

$$c_t = (\tilde{K}_H - c_H^2 - c_B c_H)(\tilde{K}_A + c_H)/c_H^2 + c_{MZ} \tag{3.16}$$

where $\tilde{K}_H \equiv K_H/\gamma_\pm^2$. From eq 3.16 one can calculate the dependence, $c_t(c_H)$; the inverse function, $c_H(c_t)$, determines the dependence of the solution's pH on the total input concentration of alkanoate, c_t. The last term in eq 3.16, c_{MZ}, is a small correction, which is given by eq 3.15. Therefore, the calculation of $c_t(c_H)$ can be carried out by iterations.

For $c_B = 0$ and $c_{MZ} \ll c_t$, eq 3.16 reduces to the respective equation in ref 4 (with $x = 0$). In the special case when $c_B = 0$, $c_H^2 \ll \tilde{K}_H$, $c_H \ll \tilde{K}_A$, and $c_{MZ} \ll c_t$, eq 3.16 yields[4]

$$pH \approx 0.5[\log(c_t) - \log(K_H\tilde{K}_A)] \tag{3.17}$$

i.e., the slope of the pH vs $\log(c_t)$ plot is +0.5.

3.3. Solutions with Precipitate of Alkanoic Acid (HZ). In this case, the concentration of the alkanoic acid is fixed:[4]

$$c_{HZ} = S_{HZ} = \text{constant} \tag{3.18}$$

where S_{HZ} is the equilibrium solubility of the acid. From eq 3.1, we express the concentration of the alkanoate ion:

$$c_Z = \frac{K_A S_{HZ}}{c_H \gamma_\pm^2} = \frac{K_{HZ}}{c_H \gamma_\pm^2} \tag{3.19}$$

(41) Fuerstenau, D. W. Thermodynamics of surfaces, adsorption, and wetting. In *Principles of Flotation*; King, R. P., Ed.; South African Institute of Mining and Metallurgy: Johannesburg, 1982; Chapter 3, pp 31−52.

(42) Robinson, R. A.; Stokes, R. H. *Electrolyte Solutions*, 2nd Ed.; Dover Publications: New York, 2002.

where $K_{HZ} \equiv K_A S_{HZ}$ is the solubility product for HZ. For lauric and myristic acids, Lucassen[4] determined $S_{HZ} = 1.05 \times 10^{-5}$ M and 5.25×10^{-7} M, respectively. Correspondingly, using the value $K_A = 1.995 \times 10^{-5}$ (ref 41) we determine the solubility product for lauric and myristic acid: $K_{HZ} = 2.09 \times 10^{-10}$ and 1.05×10^{-11}, respectively.

In the considered case, we have $m_M = 0$ and, hence, eq 3.11 is valid again. In eq 3.2, we substitute c_M from eq 3.11 and c_Z from eq 3.19. As a result, we derive the following expression for c_{MZ}:

$$c_{MZ} = \frac{c_A + c_B + c_t}{1 + Q_{MZ}\, c_H/K_{HZ}} \tag{3.20}$$

Finally, in the electroneutrality equation, eq 3.7, we substitute c_M from eq 3.11 and c_Z from eq 3.19. As a result, we obtain a quadratic equation for c_H:

$$[c_H{}^2 + (c_t + c_B - c_{MZ})c_H]\gamma_\pm{}^2 = K_t \tag{3.21}$$

$$K_t \equiv K_H + K_{HZ} \tag{3.22}$$

where K_t is a constant. In eq 3.21, c_{MZ} is a small correction, which is given by eq 3.20. Therefore, the calculation of c_H can be carried out by iterations.

For $c_B = 0$, $\gamma_\pm \approx 1$, and $c_H, c_{MZ} \ll c_t$, eq 3.21 reduces to $c_t c_H \approx K_t$, which leads to

$$\mathrm{pH} \approx \log(c_t) - \log(K_t) \tag{3.23}$$

i.e., the slope of the pH vs $\log(c_t)$ plot is +1 if a HZ precipitate is present.[4]

3.4. Solutions with Precipitate of *j*:*n* Acid Soap. If a precipitate of $(HZ)_j(MZ)_n$ acid soap is present, we have

$$\frac{m_M}{n} = \frac{m_Z}{j+n} \tag{3.24}$$

In eq 3.24, we substitute m_M and m_Z from eqs 3.9−3.10, and c_{HZ} from eq 3.1. As a result, we derive

$$c_M = \frac{j}{j+n}(c_t - c_{MZ}) + c_A + c_B + \frac{n}{j+n}\left(1 + \frac{c_H}{\tilde{K}_A}\right)c_Z \tag{3.25}$$

Next, in the electroneutrality condition, eq 3.7, we substitute c_M from eq 3.25 and obtain

$$c_Z = \hat{c}_Z - \epsilon_{jn} c_{MZ} \tag{3.26}$$

where

$$\hat{c}_Z \equiv \epsilon_{jn}[c_t - (1 + n/j)(\hat{c} - c_B)] \tag{3.27}$$

$$\epsilon_{jn} \equiv \frac{j}{j - n c_H/\tilde{K}_A}; \quad \hat{c} \equiv \frac{\tilde{K}_H}{c_H} - c_H \tag{3.28}$$

Furthermore, in eq 3.2 we substitute c_M from eq 3.7 and c_Z from eq 3.26. Neglecting quadratic terms with respect to c_{MZ}, we derive

$$c_{MZ} \approx \frac{(c_A + \hat{c} + \hat{c}_Z)\hat{c}_Z}{\tilde{Q}_{MZ} + (c_A + \hat{c} + 2\hat{c}_Z)\epsilon_{jn}} \tag{3.29}$$

The solubility relation for a precipitate of *j*:*n* acid soap reads

$$c_H{}^j c_M{}^n c_Z{}^{j+n} \gamma_\pm{}^{2j+2n} = K_{jn} \qquad (j,n = 1, 2, 3, \ldots) \tag{3.30}$$

where K_{jn} is the respective solubility product (constant). Equation 3.30, along with eqs 3.25−3.29, represents an algebraic equation for determining c_H at given c_t, c_A, and c_B.

The computational procedure is as follows. First, for a tentative value of c_H, and given c_t, c_A, and c_B, we calculate $\hat{c}_Z$, ϵ_{jn}, $\hat{c}$, and c_{MZ} from eqs 3.27−3.29. Second, from eqs 3.25 and 3.26 we calculate c_M and c_Z. Finally, the obtained values of c_M and c_Z are substituted in eq 3.30, which is solved numerically. In general, eq 3.30 has many roots for c_H and the physical root can be determined by additional considerations.

The problem becomes more complex if j, n, and K_{jn} are unknown and have to be determined by comparing theory and experiment. This difficulty can be overcome by using the method of the precipitate characteristic functions (section 4), which enables one to determine j, n, and K_{jn} without determining the roots of eq 3.30.

Simplification is possible if the concentrations of precipitates and nondissociated molecules (MZ and HZ) are negligible in comparison with the total input concentration, c_t. This is fulfilled for the NaL and NaMy solutions investigated in our experiments (section 2). In such a case, in eqs 3.9 and 3.10 we neglect m_M, m_Z, c_{MZ}, and c_{HZ} in comparison with c_t. Thus, we obtain

$$c_M \approx c_t + c_A + c_B; \quad c_Z \approx c_t \tag{3.31}$$

The substitution of c_M and c_Z from eq 3.31 into eq 3.30 yields

$$c_H{}^j (c_t + c_A + c_B)^n c_t{}^{j+n} \gamma_\pm{}^{2j+2n} \approx K_{jn} \tag{3.32}$$

Furthermore, having in mind that

$$\mathrm{pH} = -\log(c_H \gamma_\pm) \tag{3.33}$$

we obtain

$$\mathrm{pH} \approx \frac{1}{j}\log[(c_t + c_A + c_B)^n c_t{}^{j+n} \gamma_\pm{}^{j+2n}] - \frac{1}{j}\log K_{jn} \tag{3.34}$$

In the special case when there are no added salt and base ($c_A = c_B = 0$) and the ionic strength is relatively low ($\gamma_\pm \approx 1$), eq 3.34 reduces to

$$\mathrm{pH} \approx (1 + 2n/j)\log c_t - (1/j)\log K_{jn} \tag{3.35}$$

Equation 3.35 predicts that if a precipitate of *j*:*n* acid soap is present, the plot of pH vs $\log c_t$ should be a straight line of slope $1 + 2n/j$. In the case of 1:1 acid soap ($j = n = 1$), the slope is +3, as established by Lucassen.[4]

3.5. Coexistence of Precipitates of Neutral Soap and Acid Soap. If a precipitate of neutral soap (MZ) is present, then $c_{MZ} = S_{MZ} =$ constant, where S_{MZ} is the (maximum) solubility of nondissociated MZ molecules in water. Substituting $c_{MZ} = S_{MZ}$ in eq 3.2, we obtain

$$c_M c_Z \gamma_\pm{}^2 = K_{MZ} \tag{3.36}$$

where $K_{MZ} \equiv Q_{MZ} S_{MZ}$ is the solubility product for the neutral soap.

Let us assume that precipitates of acid soap and neutral soap are simultaneously present in the solution (coexistence of two solid phases). The solubility relations for the acid and neutral soaps are given by eqs 3.30 and 3.36, respectively. From the latter two equations, we determine c_Z and c_M:

$$c_Z = \left(\frac{K_{jn}}{K_{MZ}{}^n}\right)^{1/j} \frac{1}{c_H \gamma_\pm{}^2}, \quad c_M = \left(\frac{K_{MZ}{}^{j+n}}{K_{jn}}\right)^{1/j} c_H \tag{3.37}$$

The substitution of c_Z and c_M from eq 3.37 into the electroneutrality condition, eq 3.7, yields

$$a_{jn}{c_H}^2 - c_A c_H - b_{jn} = 0 \tag{3.38}$$

where

$$a_{jn} = \left(\frac{{K_{MZ}}^{j+n}}{K_{jn}}\right)^{1/j} + 1, \quad b_{jn}{\gamma_\pm}^2 = \left(\frac{K_{jn}}{{K_{MZ}}^n}\right)^{1/j} + K_H \tag{3.39}$$

In the special case $i = j = 1$, $c_A = 0$, $K_H = K_W$, and $\gamma_\pm \approx 1$, eq 3.38 reduces to eq 18 in the paper by Lucassen.[4] The physically meaningful root of eq 3.38 is

$$c_H = \frac{1}{2a_{jn}}[c_A + ({c_A}^2 + 4a_{jn}b_{jn})^{1/2}] \tag{3.40}$$

Equations 3.39 and 3.40 indicate that the pH of the respective solutions is constant, i.e., independent of the input concentration of sodium carboxylate, c_t. (A weak dependence of c_H on c_t could come through the activity coefficient, $\gamma_\pm$.) Moreover, in this case the pH is independent also of the concentration of the added base, c_B. However, the pH depends on the presence of NaCl through c_A in eq 3.40.

Next, let us consider the relative contents of acid soap and neutral soap in the two-phase precipitate. For this goal, we express the amounts of the components M and Z contained in the precipitate (per unit volume) in the form

$$m_M = m_M^{(as)} + m_M^{(ns)}, \quad m_Z = m_Z^{(as)} + m_Z^{(ns)} \tag{3.41}$$

where the superscripts (as) and (ns) denote "acid soap" and "neutral soap", respectively. In view of the chemical formulas of the two soaps, MZ and $H_jM_nZ_{j+n}$, we have

$$m_M^{(ns)} = m_Z^{(ns)} \quad \text{and} \quad (j+n)m_M^{(as)} = nm_Z^{(as)} \tag{3.42}$$

From eqs 3.41 and 3.42 we derive

$$m_Z - m_M = m_Z^{(as)} - m_M^{(as)} = \frac{j}{n}m_M^{(as)} \tag{3.43}$$

Substituting m_Z and m_M from eqs 3.9 and 3.10 into eq 3.43, we obtain

$$\frac{j}{n}m_M^{(as)} = c_M - c_Z - c_A - c_B - c_{HZ} \tag{3.44}$$

Next, we replace $c_M - c_Z - c_A$ from the electroneutrality condition, eq 3.7, c_{HZ} from eq 3.1, and c_Z from eq 3.37. As a result, eq 3.44 acquires the form

$$\frac{j}{n}m_M^{(as)} = \frac{\tilde{K}_H}{c_H} - c_H - c_B - \frac{1}{K_A}\left(\frac{K_{jn}}{{K_{MZ}}^n}\right)^{1/j} \tag{3.45}$$

Equation 3.45 shows that, in the region of coexistence of acid soap and neutral soap, the concentration of the acid-soap precipitate is constant (independent of c_t) and is determined by the value of c_H given by eq 3.40, and by the value of c_B. In particular, by increase of c_B (by addition of base) one can make the right-hand side of eq 3.45 equal to zero, which corresponds to the complete dissolution of the acid-soap precipitate. Further, having in mind that $c_{MZ} = S_{MZ}$, from eqs 3.9 and 3.41 we determine the amount of component M contained in the neutral-soap precipitate per unit volume,

$$m_M^{(ns)} = c_t + c_A + c_B - c_M - S_{MZ} - m_M^{(as)} \tag{3.46}$$

where c_M and $m_M^{(as)}$ are given by eqs 3.37 and 3.45.

In summary, eqs 3.45 and 3.46 imply that, at fixed c_A and c_B, the concentration of the *neutral*-soap precipitate *increases* linearly with c_t, whereas the concentration of the *acid*-soap precipitate remains *constant*. The addition of base (the increase of c_B) leads to increase of the neutral-soap precipitate and decrease of the acid-soap precipitate, while the pH of the solution remains constant (eq 3.40).

3.6. Solutions with Precipitate of Neutral Soap (MZ). A single precipitate of neutral soap can be observed in the presence of added base (NaOH in our experiments), when the concentrations of HZ and $(HZ)_j(MZ)_n$ become negligible.

If the only precipitate in the solution is that of MZ, then $m_M = m_Z$, and from eqs 3.9 and 3.10 we obtain

$$c_M = c_Z + c_A + c_B + c_{HZ} \approx c_Z + c_A + c_B \tag{3.47}$$

Substituting eq 3.47 into the electroneutrality condition, eq 3.7, we obtain a quadratic equation for c_H:

$${c_H}^2 + c_B c_H = \tilde{K}_H \tag{3.48}$$

Equation 3.48 indicates that if MZ precipitate is present, then c_H (and the solution's pH) is independent of the total carboxylate concentration, c_t. Moreover, if $c_H \ll c_B$, then eq 3.48 reduces to $c_H = \tilde{K}_H/c_B$, i.e., the pH of the solution is completely determined by the concentration of the added base, c_B. Substituting eq 3.47 into the solubility equation, $c_M c_Z {\gamma_\pm}^2 = K_{MZ}$, we obtain a quadratic equation for c_Z:

$${c_Z}^2 + (c_A + c_B)c_Z = K_{MZ}/{\gamma_\pm}^2 \tag{3.49}$$

From eq 3.49, we determine

$$c_Z = \frac{1}{2}\{-(c_A + c_B) + [(c_A + c_B)^2 + 4K_{MZ}/{\gamma_\pm}^2]^{1/2}\} \tag{3.50}$$

Equation 3.50 predicts that, in the presence of MZ precipitate, the bulk concentration of Z^- ions is constant (independent of c_t): $c_Z \equiv (c_Z)_{MZ} =$ constant. (A very weak concentration dependence could appear only through $\gamma_\pm$.) This result is important for the interpretation of the surface tension isotherms in Figure 3; see section 8 below.

4. Method of Precipitate Characteristic Functions

In this section we describe a method for determining the type of the precipitates in alkanoate soap solutions, and in particular, the values of j, n, and K_{jn} for the acid-soap precipitates, by theoretical analysis of the experimental data. We define the characteristic functions and indicators for each separate type of precipitate. In sections 5 and 6, we demonstrate how these characteristic functions and indicators can be applied to identify the concentration regions in which the respective precipitates exist.

4.1. Precipitate of Alkanoic (Fatty) Acid. Equation 3.21 can be presented in the form

$$f_{HZ}(c_t, c_H, c_B) = \log K_t \tag{4.1}$$

where the function f_{HZ} is equal to the log of the left-hand side of eq 3.21. Having in mind that $c_{MZ} \ll c_t$, and that $pH = -\log(c_H\gamma_\pm)$, we can represent f_{HZ} in the form

$$f_{HZ} \approx \log[(c_t + c_H + c_B)\gamma_\pm] - \text{pH} \qquad (4.2)$$

To identify the existence of a precipitate of fatty acid (HZ) in a given concentration region, one has to calculate f_{HZ} from eq 4.2 using the experimental values of c_B, c_t, and $c_H(c_t)$, and to plot f_{HZ} versus c_t. In the concentration region where a precipitate of HZ is present, the curve $f_{HZ}(c_t)$ exhibits a plateau equal to log K_t (see eq 4.1). Thus, $f_{HZ}(c_t)$ serves as a characteristic function for the HZ precipitate.

When $c_t \gg c_H$, c_B, and $\gamma_\pm \approx 1$, one could use a simpler *indicator* for HZ precipitate. As mentioned above, in this special case eqs 4.1 and 4.2 yield pH $\approx$ log c_t − log K_t. Hence, slope +1 of the plot pH vs log c_t indicates the presence of HZ precipitate.[4] The use of the more general criterion, based on eqs 4.1−4.2, gives an additional tool for identifying HZ precipitates.

4.2. Precipitate of Acid Soap, $(HZ)_j(MZ)_n$. In this case, eq 3.30 can be expressed in the form

$$f_{jn} \equiv \log(c_H^{\,j} c_M^{\,n} c_Z^{\,j+n} \gamma_\pm^{\,2j+2n}) = \log K_{jn} \qquad (4.3)$$

where $f_{jn}(c_t,c_H,c_A,c_B)$ is the characteristic function for j:n acid-soap precipitate; the functions $c_M(c_t,c_H,c_A,c_B)$ and $c_Z(c_t,c_H,c_A,c_B)$ are given by eqs 3.25−3.29. Comparing eqs 3.34 and 4.3, one obtains an approximate expression for f_{jn}:

$$f_{jn} \approx \log[(c_t + c_A + c_B)^n c_t^{\,j+n} \gamma_\pm^{\,j+2n}] - j\ \text{pH} \qquad (4.4)$$

To identify the existence of a precipitate of $(HZ)_j(MZ)_n$ acid soap in a given concentration region, one has to calculate f_{jn} in eq 4.3 or 4.4 from the experimental data for pH, c_t, c_A, and c_B, and to plot it versus c_t, assuming some test values of j and n (j, n = 1, 2, 3, ...). In the concentration region where a precipitate of j:n acid soap exists, this plot must exhibit a plateau equal to log K_{jn} (see eq 4.3).

If $c_t \gg c_A$, c_B, and $\gamma_\pm \approx 1$, one could use eq 3.35 as an *indicator* for the existence of a j:n acid-soap precipitate. According to eq 3.35, the slope of the plot pH vs log c_t is equal to $(1 + 2n/j)$, from where one could estimate j:n, i.e., the stoichiometry of the acid-soap precipitate. The use of the more general criterion based on eqs 4.3−4.4 helps one to confirm or reject the hypothesis about the formation of an acid-soap precipitate of a given stoichiometry.

4.3. Coexistence of Precipitates of Acid Soap, $(HZ)_j(MZ)_n$, and Neutral Soap, MZ. The *indicator* for coexistence of precipitates of acid and neutral soap is the constancy of pH, as predicted by eq 3.40.

In this case, the characteristic functions satisfy the following relations:

$$f_{jn} \approx \log[(c_t + c_A + c_B)^n c_t^{\,j+n} \gamma_\pm^{\,j+2n}] - j\ \text{pH} \geq \log K_{jn} \qquad (4.5)$$

$$f_{MZ} \equiv \log[(c_t + c_A + c_B) c_t \gamma_\pm^{\,2}] \geq \log K_{MZ} \qquad (4.6)$$

The simultaneous fulfillment of eqs 4.5 and 4.6 represents a necessary condition for coexistence of $(HZ)_j(MZ)_n$ and MZ precipitates.

To obtain eq 4.5, we first notice that the concentration of the Z^- ions, c_Z, is constant, independent of c_t, as it follows from eqs 3.37 and 3.40. In other words, the increase of c_t results in the formation of more precipitates at fixed c_Z. Hence, $c_t \geq c_Z$, and the replacement of c_Z by c_t in eq 4.3, along with $c_M \approx c_t + c_A + c_B$, leads to the inequality 4.5. A similar replacement of c_Z and c_M in eq 3.36 leads to the inequality 4.6.

To check whether there is coexistence of acid-soap and neutral-soap precipitates, one has to calculate $f_{jn}(c_t)$ and $f_{MZ}(c_t)$ in eqs 4.5 and 4.6 from the experimental data for pH, c_t, c_A, and c_B. It is important that the relation "=" in eqs 4.5 and 4.6 must take place at the *same* value of c_t (c_A and c_B are fixed). In the graphs $f_{jn}(c_t)$ and $f_{MZ}(c_t)$ one can easily check whether the necessary condition for coexistence of $(HZ)_j(MZ)_n$ and MZ precipitates, viz., the simultaneous fulfillment of eqs 4.5 and 4.6, is satisfied (see below).

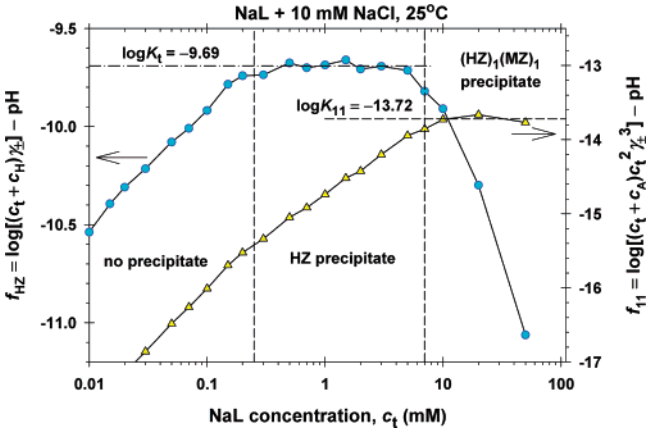

Figure 4. Plots of the precipitate characteristic functions $f_{HZ}(c_t)$ and $f_{11}(c_t)$ calculated with the help of eqs 4.2 and 4.4 using the experimental pH(c_t) dependence for NaL + 10 mM NaCl (Figure 1). The horizontal lines denote the precipitation constants determined from the plateaus of the respective curves.

5. Interpretation of the Experimental Data for NaL

5.1. Precipitation Diagram. In Figure 4, we show a precipitation diagram for NaL, which is drawn with the help of eqs 4.2 and 4.4. The functions $f_{HZ}(c_t)$ and $f_{11}(c_t)$ exhibit plateaus that indicate the presence of precipitates of HZ and 1:1 acid soap in the respective concentration regions. Note that the plateau of $f_{11}(c_t)$ begins right after the plateau of $f_{HZ}(c_t)$, with a narrow transitional zone between them. The horizontal lines (the average plateau levels) correspond to log $K_t = -9.69$ and log $K_{11} = -13.72$.

We have $K_t = K_H + K_A S_{HZ} = 10^{-9.69} = 2.04 \times 10^{-10}$ M^2; $K_H \approx 1 \times 10^{-11}$; $K_A = 1.995 \times 10^{-5}$. Then, from the above values, we calculate $S_{HZ} = 0.97 \times 10^{-5}$ M, which is close to the value given in ref 4, viz., $S_{HZ} = 1.05 \times 10^{-5}$ M.

5.2. Analysis of the Plot of pH vs log c_t. In Figure 5, the data for pH(c_t) for NaL from Figure 1 are compared with the respective theoretical curves. In accordance with the precipitation diagram in Figure 4, three concentration regions are considered.

At the lowest concentrations of NaL, its solutions do not contain precipitates. Correspondingly, we fitted the data for pH(c_t) in Figure 1 by means of eq 3.16 (with $c_B = 0$) in the concentration region $c_t < 0.25$ mM. The theoretical curve in this region is shown by solid line in Figure 5. In the calculations, we used the value $K_A = 1.995 \times 10^{-5}$ (ref 41), and from the fit we determined $K_H \approx K_{CO_2} = 1.06 \times 10^{-11}$, which coincides with its expected value $\approx 1 \times 10^{-11}$ (see above). The standard deviation of the respective theoretical curve, pH(c_t), from the experimental data is relatively small: Δ(pH) = 0.022.

In the intermediate concentration region, $0.25 < c_t < 7$ (mM), the plot of pH vs log c_t is a straight line of slope +1 (Figure 5), which indicates the formation of HZ precipitate; see eq 3.23. This fact is in agreement with the presence of a plateau in the plot $f_{HZ}(c_t)$ in Figure 4, and the value of K_t determined from Figures 4 and 5 is the same: log $K_t = -9.69$. The quality of the fit of in Figure 5, for $0.25 < c_t < 7$ (mM), is very good: the standard deviation is Δ(pH) = 0.023.

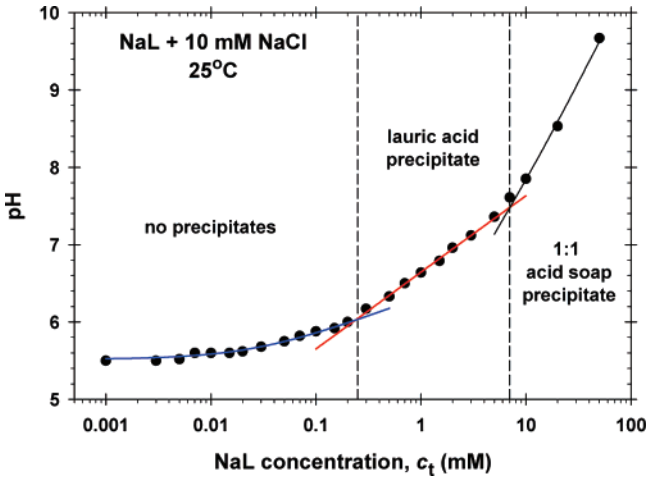

Figure 5. Plot of the experimental data for pH of NaL solutions vs the total concentration of NaL at 10 mM added NaCl. The lines are fits by the theoretical dependencies in section 3 (eqs 3.16, 3.21, and 3.34); their intersection points determine the boundaries between the zones with different precipitates shown by vertical dashed lines.

Table 1. Calculation of K_{11} by Means of Eq 5.1 (c_A = 10 mM)

c_t (M)	pH	$\gamma_\pm$	$-\log K_{11}$ (eq 5.1)
0.01	7.85	0.8712	13.73
0.02	8.53	0.8502	13.66
0.05	9.67	0.8101	13.77
			av: 13.72 ± 0.05

At the greatest NaL concentrations, $c_t > 7$ mM, the diagram in Figure 4 indicates the presence of a 1:1 acid-soap precipitate. Setting $j = n = 1$ and $c_B = 0$ in eq 3.34, we obtain

$$\mathrm{pH} \approx \log[(c_t + c_A)c_t^2\gamma_\pm^3] - \log K_{11} \qquad (5.1)$$

The theoretical line in Figure 5 for $c_t > 7$ mM is drawn by means of eq 5.1. As an illustration, in Table 1 we have listed the experimental values of c_t and pH for the three points in this region. For each point of coordinates (c_t, pH), we calculate $\gamma_\pm$ from eq 3.4 and $-\log K_{11}$ from eq 5.1. The values of $-\log K_{11}$ in the last column of Table 1, which are close to each other, visualize the applicability of eq 5.1. The average value, $-\log K_{11} = 13.72 \pm 0.05$, coincides with that for the plateau of $f_{11}(c_t)$ in Figure 4, as it should be.

In Figures 4−6, the boundaries between the regions of different precipitates, determined from the intersection points of the fits in Figure 5, are shown by vertical dashed lines.

5.3. Interpretation of the Surface Tension Isotherm. The experimental surface tension isotherm, σ vs c_t, for NaL is shown in Figure 6. First, one sees that the boundary (the vertical dashed line) between the regions without precipitates and with lauric acid precipitate, determined by analysis of the pH data in Figures 4 and 5, coincides with the first kink in the experimental surface-tension isotherm in Figure 6. Second, the experimental results for σ are insensitive to the concentration of added NaCl (Figure 6). Third, σ is almost constant in the region of lauric acid precipitate.

The above three facts could be simultaneously explained by the hypothesis that the surfactant adsorption region is composed mostly of lauric acid (HZ) in the considered concentration region ($c_t \leq 3$ mM). The respective solutions contain two amphiphiles: the nonionic HZ and the anionic Z^- (the amount of nondissociated MZ is expected to be negligible in this concentration region). It is known that even a trace amount of a nonionic amphiphile is able to displace the ionic surfactant from the surface. For example,

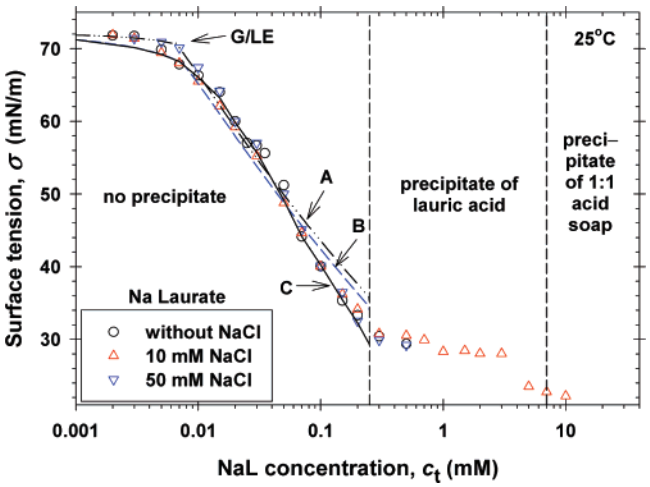

Figure 6. Comparison of different versions of the theoretical model with the experimental data. Model A: The dash−dot−dot curve is calculated assuming that only lauric acid (HZ) adsorbs. Model B: The dashed curve is calculated assuming that both lauric acid (HZ) and laurate ions (Z^-) adsorb. Model C consists in calculation of c_H from the surface tension values, rather than from the pH values, assuming adsorption of both HZ and Z^- (the continuous line). G/LE denotes the gas/liquid-expanded phase transition predicted by the van der Waals model. The vertical dashed lines are the same as in Figue 5.

in ref 43 it was demonstrated that small amounts of the nonionic dodecanol are able to significantly reduce the fraction of the anionic sodium dodecyl sulfate (SDS) in the adsorption layer. Physically, this is due to the fact that even a minor adsorption of the anionic surfactant is enough to create a high negative surface electric potential, which repels the anionic surfactant from the interface, while the subsurface concentration of the nonionic amphiphile remains equal to the bulk one.

If the interface is occupied mostly by the nonionic HZ, then the solution's surface tension should be really insensitive to the concentration of added NaCl, as it is in Figure 6. In the region without precipitates, the bulk concentration of HZ increases, which can explain the decrease of σ in this region. In the region with HZ precipitate $c_{HZ} = S_{HZ}$ = constant; correspondingly, the chemical potential of HZ and the surface tension should be constant in the latter region, as experimentally observed (Figure 6).

To quantitatively verify the hypothesis that the adsorption layer is composed mostly of HZ, we calculated the surface tension isotherm by means of the van der Waals model; see, e.g., refs 27, 43−46. This model contains several parameters. All of them have been estimated. In particular, the adsorption parameters for lauric acid are known from the fit of the surface-tension isotherm in ref 27 (see eq 6; eq 11, and Table 1 therein). For the Z^- ions, we took the values of the adsorption parameters of SDS in ref

(43) Kralchevsky, P. A.; Danov, K. D.; Kolev, V. L.; Broze, G.; Mehreteab, A. Effect of nonionic admixtures on the adsorption of ionic surfactants at fluid interfaces. 1. Sodium dodecyl sulfate and dodecanol. *Langmuir* **2003**, *19*, 5004−5018.

(44) Kralchevsky, P. A.; Danov, K. D.; Broze, G.; Mehreteab, A. Thermodynamics of ionic surfactant adsorption with account for the counterion binding: Effect of salts of various valency. *Langmuir* **1999**, *15*, 2351−2365.

(45) Kolev, V. L.; Danov, K. D.; Kralchevsky, P. A.; Broze, G.; Mehreteab, A. Comparison of the van der Waals and Frumkin adsorption isotherms for sodium dodecyl sulfate at various salt concentrations. *Langmuir* **2002**, *18*, 9106−9109.

(46) Danov, K. D.; Kralchevska, S. D.; Kralchevsky, P. A.; Ananthapadmanabhan, K. P.; Lips, A. Mixed solutions of anionic and zwitterionic surfactant (betaine). *Langmuir* **2004**, *20*, 5445−5453.

43. To compare theory and experiment, we tried three approaches, which are described consecutively below:

(*A) Only Lauric Acid (HZ) Adsorbs.* In this version of the model, there are no adjustable parameters: All parameters are known from the data fit in ref 27. The bulk concentration of HZ is determined from the pH data (Figure 5) by using eq 3.14 with $K_A = 1.995 \times 10^{-5}$. The obtained theoretical curve is shown in Figure 6 by a dash−dot−dot line. It agrees well with the experimental data, except at the higher NaL concentrations. The kink in the theoretical curve at 0.007 mM NaL corresponds to the gas/liquid-expanded (G/LE) phase transition of the lauric acid predicted by the van der Waals model.[27] The whole decrease of σ at the higher NaL concentrations is due mostly to the increase of the chemical potential of the lauric acid, HZ, because of the rise of its bulk concentration. Below, we check whether the deviation of the (dash−dot−dot) theoretical curve from the experimental points (at the greater c_t) could be attributed to the incorporation of Z^- ions in the adsorption monolayer.

(*B) Both Lauric Acid (HZ) and Laurate (Z^-) Adsorb.* In this version of the model, we involve also adsorption of Z^- in the model. The bulk concentrations, $c_Z(c_t)$ and $c_{HZ}(c_t)$, have been determined from the experimental pH(c_t) dependence (Figure 5) by means of eqs 3.13 and 3.14. The parameters of the model were specified as explained above. Again, we do not have any adjustable parameters. The obtained theoretical line, calculated by means of a procedure similar to that in section 5.2 of ref 43, is shown in Figure 6 by a dashed line. Again, there is some deviation between theory and experiment at the higher NaL concentrations. In other words, the adsorption of Z^- is small, it does not affect considerably the surface-tension isotherm, and it cannot explain the observed difference between theory and experiment at the greater concentrations. The weak effect of Z^- on σ implies also a weak effect of NaCl on σ, in agreement with the experimental results.

(*C) Bulk Concentration of HZ Determined from the Surface-Tension Data.* The difference between the experiment and theory (see above) at the higher NaL concentrations (Figure 6) could be due to inaccurate determination of the bulk HZ concentration. Indeed, if the interfacial layer consists mostly of HZ, then σ will be very sensitive to c_{HZ}, and in its own turn, c_{HZ} is sensitive to the value of pH, see eq 3.14. It turns out that a variation of pH in the frame of 0.1 (which is the reproducibility of the pH measurements) could explain the difference between theory and experiment at the greater NaL concentrations in Figure 6. For this reason, we inverted the problem: Instead of calculating σ from the pH values, we calculated pH from the σ values. The same model (and computer program) as in point B was used, but the value of pH was varied until the theoretical value of σ coincided with the experimental one. This procedure is applicable to all experimental points except those at the lowest NaL concentrations (the upper-left corner of Figure 6), where σ is close to the surface tension of pure water, and the determination of pH from the experimental σ values becomes inaccurate. (Model B was used in the latter case to draw the curves in Figure 7.) The computational procedure gives also the adsorptions of the species and the surface electric potential; see ref 43 for details.

Figure 7a shows the results for the calculated adsorptions of Z^- and HZ, Γ_Z and Γ_{HZ}, corresponding to the solid line in Figure 6, which has been obtained as explained in point C above. One sees that the adsorption of HZ steeply increases at the concentration of the G/LE surface phase transition (≈0.007 mM NaL), and then exhibits only a small increase. The adsorption of Z^- is much smaller that that of HZ. The increase of the NaCl concentration leads to some increase in Γ_Z, which is compensated by a slight decrease in Γ_{HZ}.

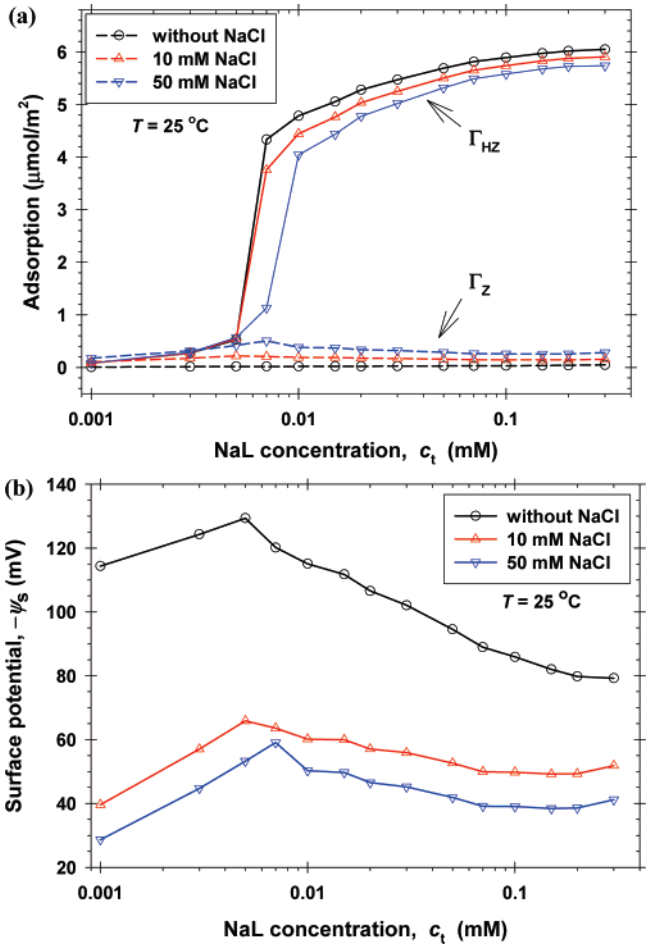

Figure 7. Theoretical curves calculated by means of model C: c_H is determined from the measured σ for the respective c_t (details in the text). (a) Adsorptions of lauric acid, Γ_{HZ}, and laurate ion, Γ_Z, vs c_t. (b) The magnitude of the surface potential, $-\psi_s$, vs c_t. The different curves correspond to different NaCl concentrations denoted in the figure.

Figure 7b shows the calculated negative surface electric potential, $-\psi_s$. In the case without NaCl, $|\psi_s|$ rises up to 130 mV, and then decreases to 80 mV because of the increasing ionic strength due to the NaL. It is not surprising that at low values of the ionic strength, I, a small adsorption of Z^- may lead to a relatively high surface potential. Such behavior is predicted by the Gouy equation[47] (the relation between surface charge and surface potential). In addition, the magnitude of the surface potential decreases with the rise of the NaCl concentration (Figure 7b). This is the well-known effect of suppression of the electric double layer by the added electrolyte.[48] To check the reliability of the calculated ψ_s, we carried out a control experiment: We measured the thickness of a free foam film formed from a solution of $c_t = 0.2$ mM NaL with $c_A = 10$ mM NaCl. The measured thickness of ≈24 nm coincides (in the framework of the experimental accuracy) with the value calculated by means of the DLVO theory[48] with $\psi_s \approx -50$ mV (Figure 7b).

(47) Davies, J. T.; Rideal, E. K. *Interfacial Phenomena*; Academic Press: London, 1963.
(48) Israelachvili, J. N. *Intermolecular and Surface Forces*; Academic Press: London, 1992.

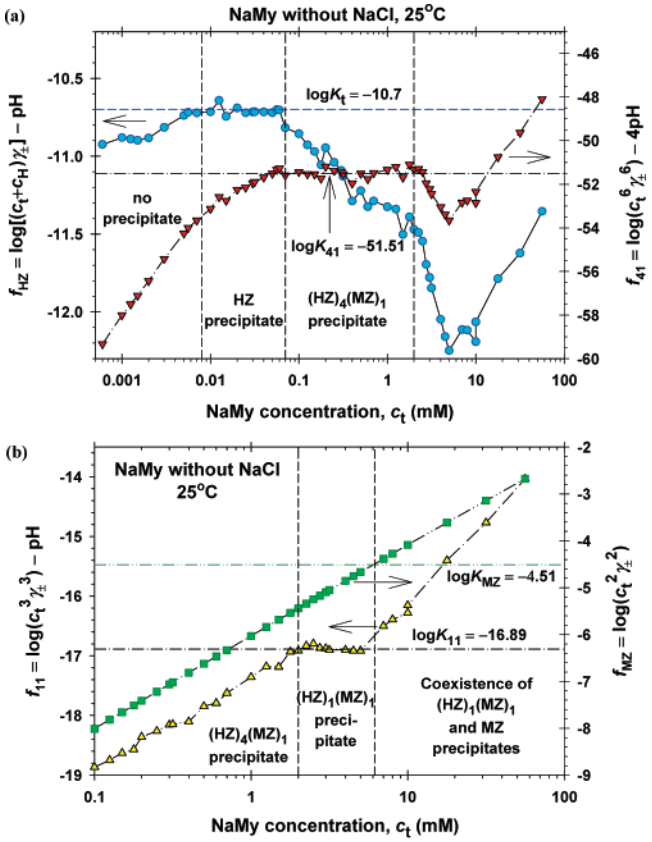

Figure 8. Precipitation diagrams for solutions of NaMy without added NaCl. (a) Plots of $f_{HZ}(c_t)$ and $f_{41}(c_t)$. (b) Plots of $f_{11}(c_t)$ and $f_{MZ}(c_t)$. These characteristic functions are calculated from eqs 4.2, 4.4, and 4.6 using the experimental pH(c_t) dependence. The vertical dashed lines denote the boundaries between the concentration regions with different precipitates. The horizontal lines denote the precipitation constants determined from the plateaus of the respective curves.

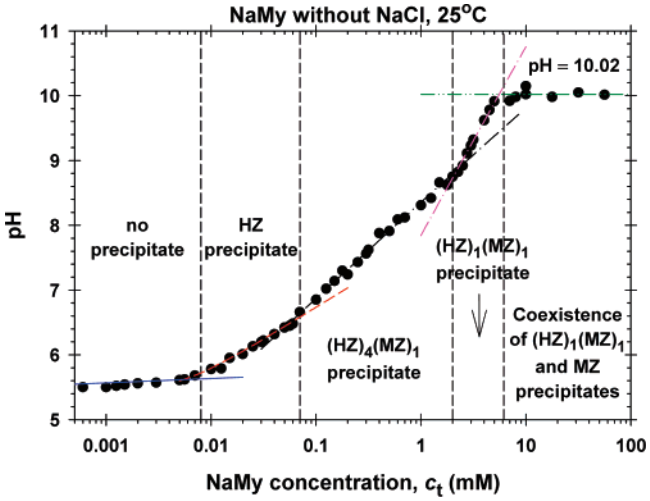

Figure 9. Plot of the experimental data for pH of NaMy solutions (no added NaCl) vs the total concentration of NaMy. The lines are fits by the theoretical dependencies (eqs 3.16, 3.21, and 3.34, the latter for j:n = 4:1 and 1:1). Their intersection points determine the boundaries between the zones with different precipitates shown by vertical dashed lines.

6. Interpretation of the Experimental Data for NaMy

6.1. Solutions of NaMy without Added NaCl. In Figure 8a, we show the plots of the functions $f_{HZ}(c_t)$ and $f_{41}(c_t)$ calculated from the experimental data for pH by means of eqs 4.2 and 4.4 ($c_A = c_B = 0$). $f_{HZ}(c_t)$ exhibits a plateau in the zone of HZ precipitate, $0.008 < c_t < 0.07$ (mM). In the region $0.07 < c_t < 2$ (mM), the plot of the experimental pH vs c_t has a slope equal to 3/2 (Figure 9) which corresponds to a precipitate of 4:1 acid soap in accordance with eq 3.35. The presence of such a precipitate is confirmed by the plot of f_{41} vs c_t, which exhibits a plateau in the respective concentration region (Figure 8a). From the average value of f_{41} in the plateau region, we determine log $K_{41} = -51.51$.

Note that the plateau of f_{41} begins at the end of the plateau of f_{HZ} ($c_t = 0.07$ mM), and ends at the beginning of the plateau of f_{11} ($c_t = 2$ mM; Figure 8b). The latter indicates the presence of 1:1 acid-soap precipitate in the region $2 < c_t < 6.15$ (mM). The average value of f_{11} at its plateau is log $K_{11} = -16.89$ (for 1:1 acid soap of NaMy). The latter value is close to −16.8 determined by Lucassen[4] for 1:1 acid soap of potassium myristate (KMy).

The end of the plateau of f_{11} (Figure 8b) corresponds to the same concentration ($c_t = 6.15$ mM) at which the curve $f_{MZ}(c_t)$ intersects the constant line log $K_{MZ} = -4.51$. The latter value agrees with the positions of the lower boundary of the zone with two solid-phase precipitates in all diagrams presented in this article (see below). In particular, Figure 8b shows that, for $c_t >$ 6.15 mM, eqs 4.5 and 4.6 are simultaneously satisfied, which indicates the coexistence of 1:1 acid soap with MZ precipitates. This is confirmed by the plateau of the curve in Figure 9 corresponding to pH = 10.02. The latter experimental value agrees well with the value pH = 10.1, which is predicted by eq 3.40 (along with eq 3.39) for $j = n = 1$; $c_A = 0$; log $K_{MZ} = -4.51$; log $K_{11} = -16.89$; $\gamma_\pm = 0.916$ ($I = 7$ mM), and $K_H = K_W = 6.81 \times 10^{-15}$.

As established earlier,[49] the plot of the electric conductance of NaMy solutions vs the NaMy concentration exhibits a kink at $c_t = 6-7$ mM. We also carried out conductance measurements and confirmed the presence of such a kink. According to the interpretation of the data in Figures 8b and 9, this kink coincides with the threshold concentration for formation of coexisting precipitates of NaMy and 1:1 acid soap.

6.2. Solutions of NaMy + 10 mM NaCl. In Figure 10, we have plotted the characteristic functions $f_{HZ}(c_t)$ and $f_{32}(c_t)$, calculated from eqs 4.2 and 4.4 ($c_A = 10$ mM, $c_B = 0$). The term c_{MZ} in eqs 3.16 and 3.21 is negligible in comparison with c_t, and therefore the solution's pH is independent of the concentration of added NaCl in the concentration regions without precipitate and with HZ precipitate. For this reason, the boundary between the latter two regions (at $c_t = 0.008$ mM) in Figure 10a is the same in Figure 8a.

We checked the behavior of the various characteristic functions $f_{jn}(c_t)$, $j,n = 1, 2, 3, ...$, in the zone of acid-soap precipitate. This analysis showed the presence of 3:2 and 1:1 acid-soap precipitates at the lower and higher NaMy concentrations, respectively. In particular, $f_{32}(c_t)$ has a plateau corresponding to log $K_{32} = -45.0$ for $0.04 < c_t < 0.3$ mM (Figure 10a), while $f_{11}(c_t)$ exhibits a plateau at log $K_{11} = -16.89$ for $0.3 < c_t < 2.9$ mM (Figure 10b).

As seen in Figure 10b, for $c_t > 2.9$ mM, both eqs 4.5 (for $j = n = 1$) and 4.6 are satisfied, and consequently, we are dealing with coexistence of 1:1 acid-soap and MZ precipitates. In addition, Figure 11a shows that in this concentration region we have pH = 9.85 = constant, which is an indicator for the coexistence of two precipitates. The latter experimental value agrees well with the value pH = 9.81, which is predicted by eq 3.40 (along with

(49) Campbell, A. N.; Lakshminarayanan, G. R. Conductances and surface tensions of aqueous solutions of sodium decanoate, sodium laurate and sodium myristate at 25° and 35°. *Canadian J. Chem.* **1965**, *43*, 1729−1737.

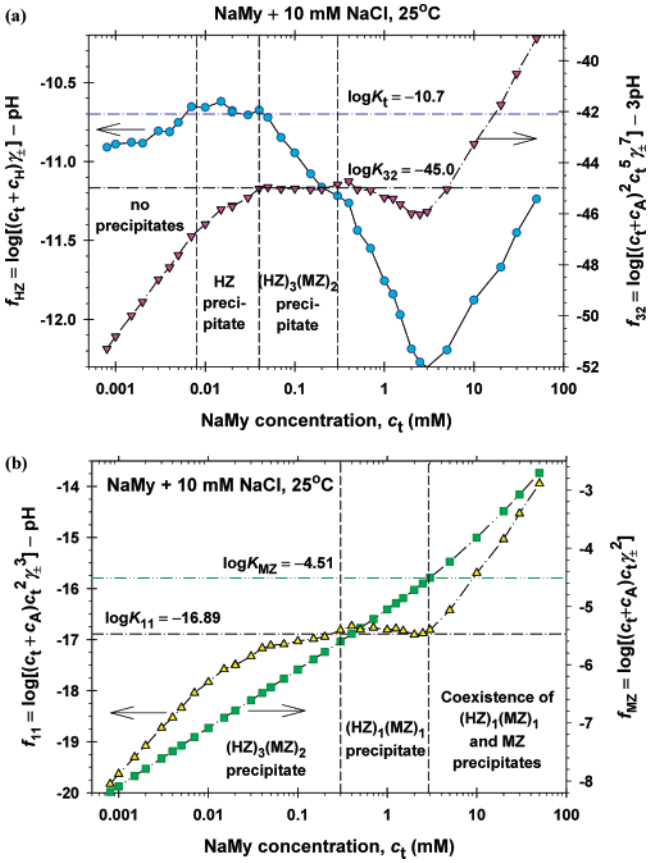

Figure 10. Precipitation diagrams for solutions of NaMy with 10 mM added NaCl. (a) Plots of $f_{HZ}(c_t)$ and $f_{32}(c_t)$. (b) Plots of $f_{11}(c_t)$ and $f_{MZ}(c_t)$. These characteristic functions are calculated from eqs 4.2, 4.4, and 4.6, using the experimental pH(c_t) dependence. The vertical dashed lines denote the boundaries between the concentration regions with different precipitates. The horizontal lines denote the precipitation constants determined from the plateaus of the respective curves.

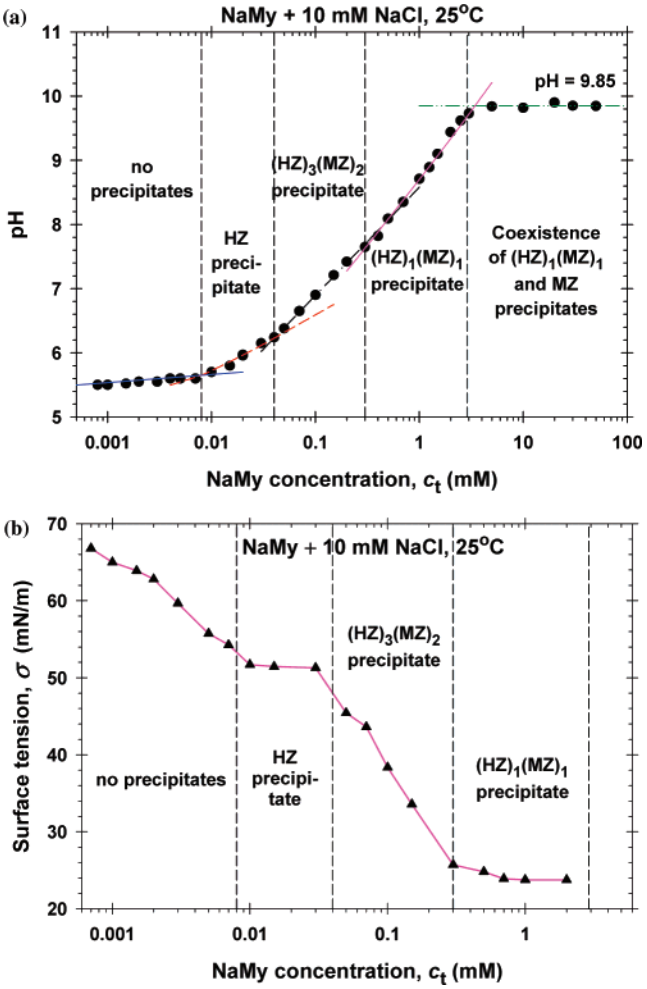

Figure 11. (a) Plot of the experimental data for pH of NaMy solutions vs the total concentration of NaMy at 10 mM added NaCl. The lines are fits by the theoretical dependencies (eqs 3.16, 3.21, and 3.34, the latter for j:n = 3:2 and 1:1). Their intersection points determine the boundaries between the zones with different precipitates shown by vertical dashed lines. (b) Comparison of the experimental surface-tension isotherm with the precipitation zones determined from the pH data.

eq 3.39) for $j = n = 1$; $c_A = 10$ mM; $\log K_{MZ} = -4.51$; $\log K_{11} = -16.89$; $\gamma_\pm = 0.879$ ($I = 17$ mM), and $K_H = K_W = 6.81 \times 10^{-15}$.

In Figure 11b we compare the boundaries between the different precipitation regions (determined from the pH data in Figures 10 and 11a) with the surface-tension isotherm of NaMy with 10 mM NaCl (Figure 2). The isotherm (Figure 11b) exhibits two plateau regions. The first plateau, at $\sigma \approx 51.5$ mN/m, corresponds to the region of HZ precipitate. The constancy of σ indicates that in this concentration zone the surface adsorption layer is composed mostly of myristic acid (HZ), whose chemical potential is constant if HZ precipitates are present in the solution. The second plateau, at $\sigma = 24-26$ mN/m, is in the region of the 1:1 acid-soap precipitate. In this concentration region, the bulk chemical potential of the 1:1 acid soap is constant, and the constancy of σ indicates that the adsorption layer could represent a monolayer of 1:1 acid soap. In the intermediate concentration zone, $0.04 < c_t < 0.3$ (mM), where 3:2 acid-soap precipitate is present in the bulk, σ undergoes a decrease with about 27 mN/m, which most probably corresponds to a transition in the composition of the adsorption monolayer from almost pure myristic acid to a monolayer of 1:1 acid soap.

Another interesting aspect of Figure 11b is that the surface tension of the solutions is determined by the bulk NaMy concentration, irrespective of the fact that the myristic acid and acid soaps have a very low solubility in the aqueous phase, so that they are often considered as water-insoluble components. The reason for the bulk-surface equilibration could be the presence of the soluble myristate ion, Z^-, which can be exchanged between the bulk and the interface. Having once adsorbed, the Z^- ion could undergo a transformation into HZ, or could be incorporated into an acid-soap complex in the adsorption monolayer.

6.3. Solutions of NaMy + 100 mM NaCl. The respective precipitation diagram is shown in Figure 12a, where we have plotted the characteristic functions $f_{HZ}(c_t)$ and $f_{11}(c_t)$, calculated from eqs 4.2 and 4.4 ($c_A = 100$ mM, $c_B = 0$). The plateau of f_{HZ} at the lowest concentrations, $c_t \le 0.02$ mM, indicates the formation of myristic acid precipitate in that concentration domain. At higher concentrations, $0.02 \text{ mM} \le c_t \le 0.5$ mM, f_{11} exhibits a broad plateau, corresponding to the concentration zone with precipitate of 1:1 acid soap. At this plateau, $f_{11} \equiv \log K_{11} = -16.89$, which is the same as for the independent sets of experimental data plotted in Figures 8b and 10b for the solutions with 0 and 10 mM NaCl.

As seen in Figure 12b, for $c_t > 0.5$ mM, both eqs 4.5 (for $j = n = 1$) and 4.6 are satisfied, and consequently, we are dealing with coexistence of 1:1 acid soap and MZ precipitates. In addition, Figure 13 shows that in this concentration region we have pH = 8.87 = constant, which also indicates the coexistence of two precipitates. The latter experimental value is close to the value

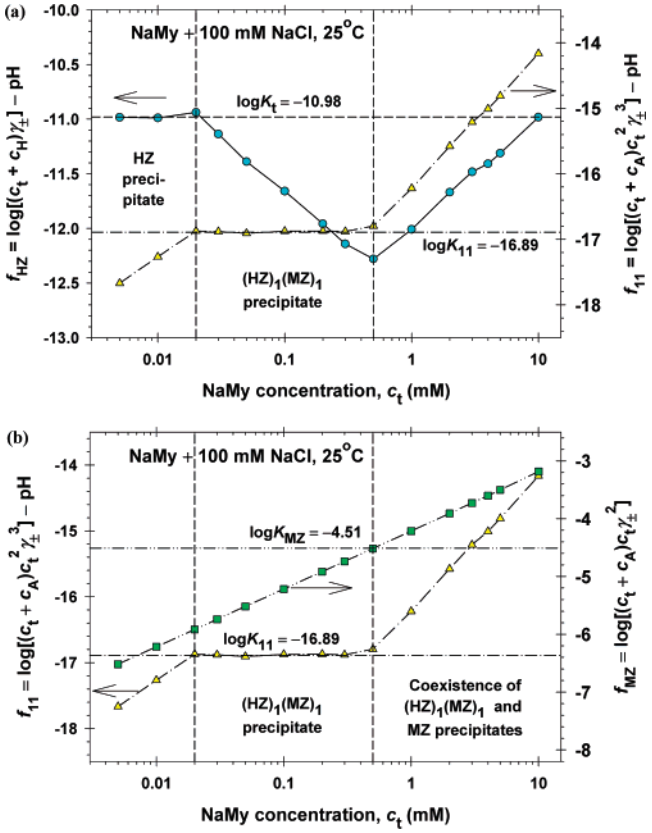

Figure 12. Precipitation diagrams for solutions of NaMy with 100 mM added NaCl. (a) Plots of $f_{HZ}(c_t)$ and $f_{11}(c_t)$. (b) Plots of $f_{11}(c_t)$ and $f_{MZ}(c_t)$. These characteristic functions are calculated from eqs 4.2, 4.4, and 4.6, using the experimental pH(c_t) dependence. The vertical dashed lines denote the boundaries between the concentration regions with different precipitates. The horizontal lines denote the precipitation constants determined from the plateaus of the respective curves.

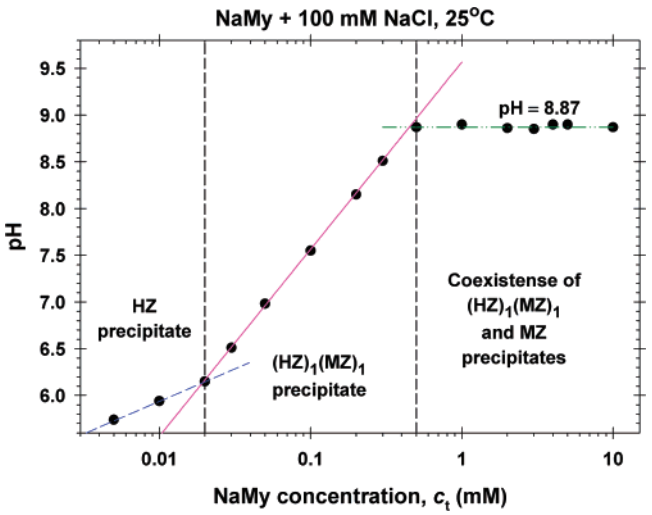

Figure 13. Plot of the experimental data for pH of NaMy solutions vs the total concentration of NaMy at 100 mM added NaCl. The lines are fits by the theoretical dependencies (eqs 3.21, and 3.34, the latter for j:n = 1:1). Their intersection points determine the boundaries between the zones with different precipitates shown by vertical dashed lines.

pH = 8.98, which is predicted by eq 3.40 (along with eq 3.39) for $j = n = 1$; $c_A = 100$ mM; log $K_{MZ} = -4.51$; log $K_{11} = -16.89$; $\gamma_\pm = 0.773$ ($I \approx 100$ mM), and $K_H = K_W = 6.81 \times 10^{-15}$.

6.4. Discussion. We have to mention that the precipitation zones in Figures 5, 9, 11a, and 13, whose boundaries have been determined by theoretical analysis of the data, agree well with the experimental observations. In particular, in the region of lowest concentrations, denoted by "no precipitate" in the figures, experimentally one observes that the solutions are clear and transparent, without any precipitates. In the zone with HZ precipitate, the solutions are opalescent. In the zones with acid-soap precipitates, the solutions contain crystallites, which can be seen by optical microscopy. For example, in the zone with 1:1 acid soap (Figure 9) the solutions contain platelike crystallites (Figure 14a). With time, they form sediment at the bottom of the vessel. Finally, in the zone of two solid phases one observes two types of crystallites: platelike and fiberlike (see Figure 14b). At higher concentrations, the interweaving of the fibers results in the formation of gel-like "lumps". The addition of 10 mM NaOH leads to disappearance of the platelike crystals, while the fiberlike ones remain (see section 8.1). Most probably, the platelike crystals represent 1:1 acid soap, while the fiberlike ones represent neutral soap (MZ).

In principle, it is possible to separate the precipitate and to analyze it. For example, one can use IR spectroscopy.[3] As established here (Figures 9 and 11a), the stoichiometry of the crystallites could change during the evaporation of water (increase of c_t) when obtaining solid samples. The change of stoichiometry can be avoided by a quick removal of the formed crystals from the solution. Such analytical investigation could be a subject of a subsequent study.

Another issue that deserves to be discussed is related to the possibility for micellization in the investigated alkanoate solutions. At 25 °C, the lauric and myristic acids have an extremely low solubility in water, and therefore, they form crystallites in the solutions at very low concentrations, at which formation of micelles is not expected. If we assume that micelles appear at higher concentrations, they should form at the background of already formed crystallites (the presence of crystallites is directly seen by optical microscope in the investigated solutions). It is practically impossible to *directly* detect the presence of micelles, e.g., by light scattering, on the background of the powerful signal from the bigger crystallites. However, it is possible to detect the effect of the micelles *indirectly*, from the measured pH. In accordance with the Gibbs phase rule, the appearance of micelles, which coexist with a solid precipitate, would reduce the thermodynamic degrees of freedom by one.[4] Theoretically, this results in the appearance of an additional equation; see eq 15 in ref 4. The latter represents the known relation between the CMC and the counterion concentration (the CMC decreases with the rise of counterion concentration, the dependence being linear in log−log scale). This equation leads to a negative slope in the concentration dependence of pH,[4] which is not observed in the solutions of NaL and NaMy (at 25 °C) investigated by us; see Figures 5, 9, 11a, and 13. However, in principle it is possible for the MZ crystals to be converted into MZ micelles at higher temperatures, or upon change of the counterion (K^+ instead of Na^+). In general, the problem about the coexistence of crystallites and surfactant micelles in the carboxylate soap solutions demands additional investigations.

7. Solubility Products of the Acid Soaps

The values of the constants K_{jn} for NaMy, determined from the precipitation diagrams in Figures 8, 10, and 12, are listed in Table 2.

Here, our purpose is to analyze the dependence of K_{jn} on j and n. For this goal, let us first consider the chemical-equilibrium

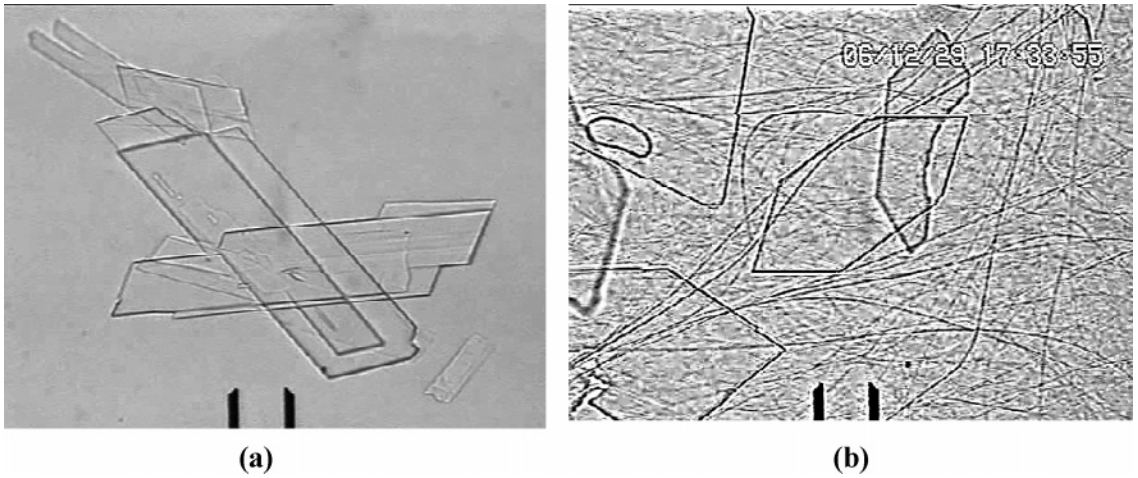

Figure 14. Photographs of crystallites in solutions of NaMy without added NaCl, at 25 °C. (a) Platelike crystallites are seen in the solutions of 4 mM NaMy (region of 1:1 acid soap); mark = 20 μm. (b) Platelike and fiberlike crystallites are observed in the solutions of 10 mM NaMy (region of coexistence of 1:1 acid soap and neutral soap); mark = 16 μm.

Table 2. Solubility Products for Precipitates in NaMy Solutions

solubility product, K_{jn}
$\log K_{MZ} = -4.51 \pm 0.05$
$\log K_{11} = -16.89 \pm 0.08$
$\log K_{32} = -44.99 \pm 0.26$
$\log K_{41} = -51.51 \pm 0.37$

Table 3. Calculation of *Y* from the Data in Table 2 for NaMy

j:*n*	$\eta = j/n$	$-\log K_\eta$	*Y*
1:1	1	16.89	16.89
3:2	1.5	22.50	22.09
4:1	4	51.51	50.53

Table 4. Calculation of K_{MZ} from the Kinks in Figure 3 (c_B = 10 mM)

c_A (mM)	$c_{t,kink}$ (mM)	$\gamma_\pm$ (eq 3.4)	$-\log K_{MZ}$ (eq 8.2)
0	3.0	0.8913	4.51
20	1.4	0.8477	4.50
100	0.5	0.7726	4.48
			av: 4.50 ± 0.1

relation for *j*:*n* acid-soap crystallites in a carboxylate soap solution:

$$j\mu_H + n\mu_M + (j+n)\mu_Z = \mu_{jn}^{(s)} \qquad (7.1)$$

Here, μ_H, μ_M, and μ_Z are the chemical potentials of the H^+, M^+, and Z^- ions in the aqueous phase; $\mu_{jn}^{(s)}$ is the chemical potential of the *j*:*n* acid-soap complex in the solid phase. The expressions for the chemical potentials of the ions in the solution are

$$\mu_X = \mu_X^{(0,l)} + kT\ln(c_X\gamma_\pm) \qquad (7.2)$$

X = H, M, Z; $\mu_X^{(0,l)}$ is the standard chemical potential of the respective component in the liquid phase; *k* is the Boltzmann constant; *T* is temperature. Substituting eq 7.2 for X = H, M, and Z into eq 7.1, we obtain the solubility relation for the *j*:*n* acid soap, $c_H{}^j c_M{}^n c_Z{}^{j+n}\gamma_\pm{}^{2j+2n} = K_{jn}$, with

$$kT\ln K_{jn} = \mu_{jn}^{(s)} - j\mu_{HZ}^{(0,l)} - n\mu_{MZ}^{(0,l)} \qquad (7.3)$$

where we have introduced the notation

$$\mu_{HZ}^{(0,l)} \equiv \mu_H^{(0,l)} + \mu_Z^{(0,l)}, \quad \mu_{MZ}^{(0,l)} \equiv \mu_M^{(0,l)} + \mu_Z^{(0,l)} \qquad (7.4)$$

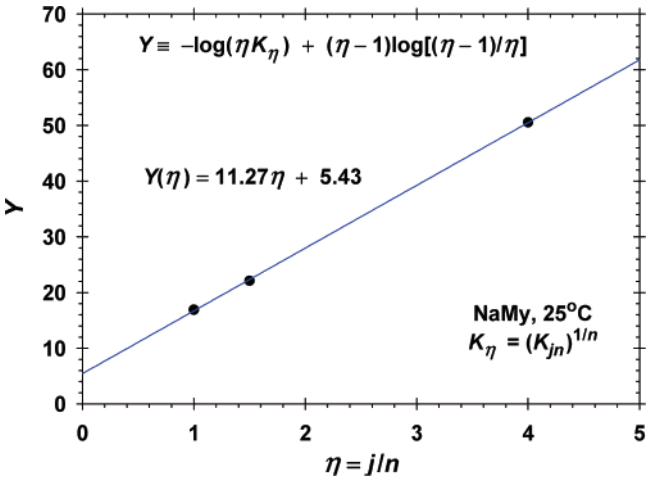

Figure 15. Plot of *Y* vs η (Table 3) in accordance with eq 7.11. The straight line, whose equation is shown in the figure, is the best fit by linear regression.

In the special case $j = n = 1$, eq 7.3 reduces to

$$kT\ln K_{11} = \mu_{11}^{(0,s)} - \mu_{HZ}^{(0,l)} - \mu_{MZ}^{(0,l)} \qquad (7.5)$$

where $\mu_{11}^{(0,s)}$ is the standard chemical potential of a molecule of 1:1 acid soap in a crystallite of of 1:1 acid soap. Likewise, one could derive the solubility relation for the crystallites of alkanoic acid, $c_H c_Z \gamma_\pm{}^2 = K_{HZ}$, with

$$kT\ln K_{HZ} = \mu_{HZ}^{(0,s)} - \mu_{HZ}^{(0,l)} \qquad (7.6)$$

where $\mu_{HZ}^{(0,s)}$ is the standard chemical potential of a HZ molecule in a crystallite of pure component HZ.

In our experiments we observed only acid soaps with $j \geq n$. In this case, the solid phase of $(HZ)_j(MZ)_n$ acid soap can be modeled as an ideal solid solution of 1:1 acid soap, $(HZ)_1(MZ)_1$, and alkanoic acid, HZ:

$$\mu_{jn}^{(s)} = n\mu_{11}^{(s)} + (j-n)\mu_{HZ}^{(s)} \qquad (j \geq n) \qquad (7.7)$$

where

$$\mu_{11}^{(s)} = \mu_{11}^{(0,s)} + kT\ln x_{11}, \quad \mu_{HZ}^{(s)} = \mu_{HZ}^{(0,s)} + kT\ln x_{HZ} \qquad (7.8)$$

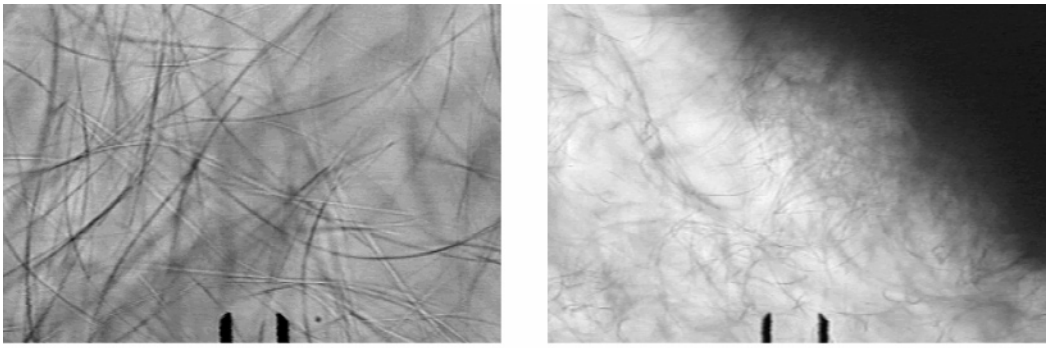

Figure 16. Photographs of crystallites formed in solutions of NaMy in the presence of 10 mM NaOH. (a) At 5 mM NaMy, fiberlike crystallites are observed (mark = 20 μm). (b) At 10 mM NaMy, the fibers form bigger "lumps"; the edge of such a lump is seen (mark = 100 μm).

x_{11} and x_{HZ} are the molar fractions of the 1:1 acid soap and HZ, respectively, in the solid phase of *j*:*n* acid soap:

$$x_{11} = \frac{n}{j} \quad \text{and} \quad x_{HZ} = \frac{j-n}{j} \tag{7.9}$$

Further, in eq 7.3 we substitute $\mu_{jn}^{(s)}$ from eq 7.7 (along with eq 7.8), and after that we replace $\mu_{11}^{(0,s)}$ and $\mu_{HZ}^{(0,s)}$ from eqs 7.5 and 7.6. After some transformations, we derive

$$\log K_{jn} = n \log(x_{11}K_{11}) + (j-n)\log(x_{HZ}K_{HZ}) \qquad (j \geq n) \tag{7.10}$$

Equation 7.10 can be represented in the following equivalent form:

$$Y(\eta) = \eta(-\log K_{HZ}) + \log(K_{HZ}/K_{11}) \tag{7.11}$$

where

$$Y \equiv -\log(\eta K_\eta) + (\eta - 1)\log\left(\frac{\eta - 1}{\eta}\right) \qquad (\eta \geq 1) \tag{7.12}$$

$$\eta \equiv \frac{j}{n}, \quad K_\eta \equiv (K_{jn})^{1/n}, \quad x_{11} = \frac{1}{\eta}, \quad x_{HZ} = \frac{\eta - 1}{\eta} \tag{7.13}$$

Using the data in Table 2, we calculated η, K_η, and Y for the investigated acid soaps of different stoichiometry; see Table 3.

In Figure 15, the data in Table 3 are plotted as Y vs η. One sees that the experimental points comply well with a straight line, in accordance with eq 7.11. The slope of the linear regression gives $\log K_{HZ} = -11.27 \pm 0.14$, which is close to the estimate $\log K_{HZ} = \log(K_A S_{HZ}) \approx -11.0$ obtained from the values of K_A and S_{HZ} in section 3.3.

On the one hand, the *intercept* of the linear regression (Figure 15) is 5.43 ± 0.34. On the other hand, taking the value $\log K_{HZ} = -11.27$ obtained from the *slope*, and $\log K_{11} = -16.89$ from Table 2, we calculate that the intercept should be $\log(K_{HZ}/K_{11}) = 16.89 - 11.27 = 5.62$; see eq 7.11. The values of the intercept obtained in these two different ways coincide in the framework of the experimental accuracy, which implies that the considered model is self-consistent.

The obtained results indicate that the model proposed in the present section could be used to estimate the value of K_{jn} for acid-soap crystallites of various *j* and *n* ($j \geq n$) formed in solutions of sodium myristate. For this purpose, one can use eqs 7.9−7.10 with $\log K_{11} = -16.89$ and $\log K_{HZ} \approx -11.27$. Equations 7.9−7.10 could be also applied to potassium myristate using the values of K_{11} and K_{HZ} determined in ref 4.

Likewise, for $n \geq j$ one could model the acid soaps as solid solutions of 1:1 acid soap and MZ. The expressions resulting from the latter model can be obtained by formal replacements HZ→MZ; *j*→*n*, and *n*→*j* in eq 7.9, and in the right-hand side of eq 7.10.

8. Surface Tension of NaMy Solutions Containing 10 mM NaOH: Interpretation

8.1. Interpretation of the Isotherms' Kinks. As mentioned in section 3.6, in the presence of 10 mM NaOH (pH ≈ 12) the concentrations of myristic acid and acid soap in the NaMy solutions are negligible. The expected type of precipitate in such solutions is that of neutral soap (MZ). Below, we check whether it is possible for the kinks in the surface-tension isotherms in Figure 3 to be due to the appearance of MZ precipitate. At concentrations greater that those of the kinks, one really observes the formation of crystallites, which have the shape of fibers (Figure 16a). At higher concentrations, these fibers exhibit the tendency to aggregate into bigger "lumps" (Figure 16b).

Let us denote by $c_{t,kink}$ the value of c_t corresponding to the kink in the surface-tension isotherm, $\sigma(c_t)$; see Figure 3. If the kink represents the onset of MZ-precipitate formation, then

$$c_Z = c_t \quad \text{for} \quad c_t < c_{t,kink}$$
$$c_Z < c_t \quad \text{for} \quad c_t > c_{t,kink} \tag{8.1}$$

At the kink, itself, we have $c_Z = c_{t,kink}$, and we can use eq 3.49 to calculate K_{MZ}:

$$K_{MZ} = (c_{t,kink} + c_A + c_B)c_{t,kink}\gamma_\pm^2 \tag{8.2}$$

In Table 4, we present the experimental values of $c_{t,kink}$ for the three curves in Figure 3, and the respective values of K_{MZ} calculated by means of eq 8.2.

One sees that the values of $\log K_{MZ}$ (Table 4), calculated for three different surface tension isotherms, are practically identical and, moreover, they coincide with the value $\log K_{MZ} = -4.51 \pm 0.05$ independently determined from the precipitation diagrams in Figures 8b, 10b, and 12b; see also Table 2. This coincidence confirms the hypothesis that the kinks in the surface tension isotherms in Figure 3 correspond to the threshold concentration for the appearance of neutral soap (MZ) precipitate. In such a case, the constancy of the surface tension at $c_t > c_{t,kink}$ (Figure 3), where the chemical potential of the MZ molecules should be constant, indicates that the surfactant adsorption monolayer is composed mostly of MZ.

Figure 17 shows experimental data for the electric conductivity of NaMy solutions with 10 mM NaOH (no added NaCl). After

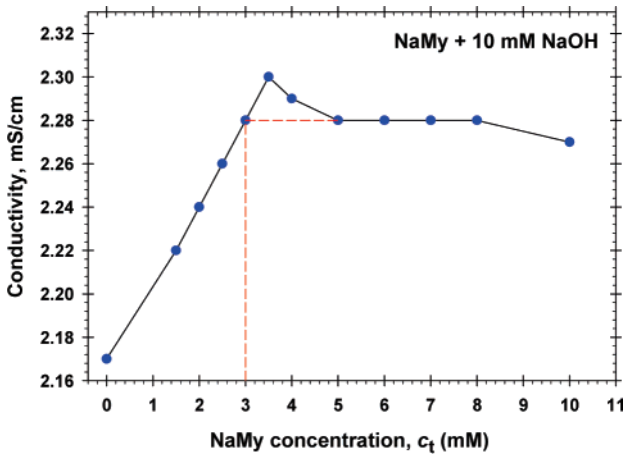

Figure 17. Plot of the electric conductivity of NaMy solutions with 10 mM added NaOH. The conductivity increases in the region without precipitates, but levels off in the zone with MZ precipitate. The solid line is a guide to the eye. The "horn" of the graph is due to supersaturation. The extrapolation of the plateau (the dashed line) gives the threshold concentration for precipitation (c_t = 3 mM); compare with the kink in Figure 3.

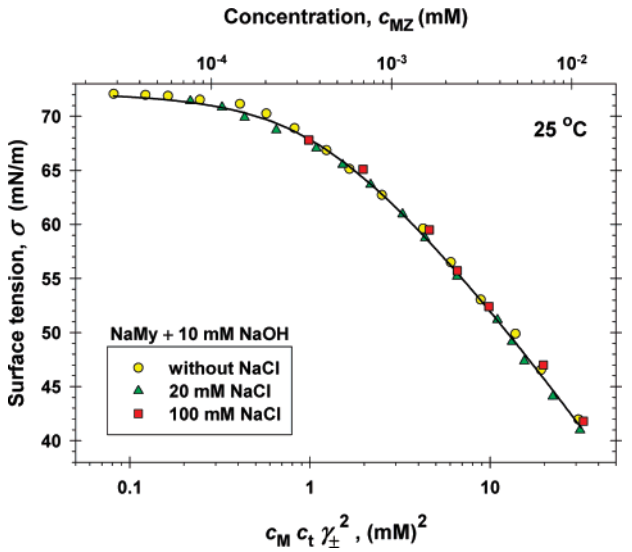

Figure 18. The three experimental curves in Figure 3 merge when σ is plotted vs $c_M c_t \gamma_\pm^2$. The solid line is the theoretical fit of the data (section 8.2); $c_{MZ} = c_M c_t \gamma_\pm^2/Q_{MZ}$ is the concentration of nondissociated NaMy in the solutions; Q_{MZ} = 2.84 M is determined from the fit.

the equilibrations of the solutions for 24 h at 25 °C, the solutions were subjected to centrifugation for 1 h at 5000 rpm to separate the crystallites (like those in Figure 16) and then the conductivity of the separated liqueur was measured. In the region without precipitates the conductivity linearly increases, whereas for $c_t \geq$ 5 mM the conductivity levels off (Figure 17). The latter fact indicates that surfactant micelles are missing in the plateau region. As mentioned above, the constancy of surface tension in this concentration region (Figure 3) could be explained by the formation of MZ crystallites.

8.2. Interpretation of $\sigma(c_t)$ at Concentrations below the Kinks. The portions of the curves in Figure 3 at $c_t < c_{t,kink}$ are plotted in Figure 18 vs the product $c_M c_Z \gamma_\pm^2$. (In this concentration region $c_Z = c_t$; see eq 8.1) One sees that the three different experimental curves coincide in Figure 18. We checked several possible explanations of this fact. The most probable of them is that a small amount of nondissociated neutral-soap (MZ) molecules exists in these solutions. Its dissociation equilibrium is described by eq 3.2. The MZ molecules behave as a nonionic surfactant. As discussed in section 5.3 and ref 43, a nonionic amphiphile of concentration about 1% of that of the ionic surfactant (which is repelled by the similarly charged interface) is sufficient to displace almost completely the ionic surfactant from the adsorption layer. In such a case, the surface tension, σ, would be governed solely by c_{MZ}, which is proportional to the product $c_M c_Z \gamma_\pm^2$, as indicated by eq 3.2. This explains the merging of the three experimental curves in Figure 18.

We tried to fit the experimental isotherms in Figure 3 by means of the detailed (two-component) van der Waals model,[43] which assumes adsorption of both MZ and Z^-. As usual, the least-squares method was applied. The adsorption constants of the two surfactants were varied as adjustable parameters. Under normal conditions, the merit function has a minimum, which corresponds to the best fit that determines the values of the adsorption constants.[43] However, for the data in Figure 3 it turns out that the merit function has no minimum with respect to the adsorption constants of Z^-. (A "valley" was observed, instead of a local minimum.) These constants cannot be determined from the data for σ, because the effect of Z^- on σ is negligible.

In such a case, there is no other choice but to consider the adsorption layer as being composed of the nonionic MZ alone, and to apply the single-component van der Waals model. The two basic equations of this model,[27,43−45] adapted to the considered case, are

$$\sigma_0 - \sigma = \frac{\Gamma kT}{1 - \alpha\Gamma} - \beta\Gamma^2 \tag{8.3}$$

$$Kc_{MZ} = \frac{\alpha\Gamma}{1 - \alpha\Gamma} \exp\left(\frac{\alpha\Gamma}{1 - \alpha\Gamma} - \frac{2\beta\Gamma}{kT}\right) \tag{8.4}$$

Here σ_0 is the surface tension of pure water; Γ is the adsorption of MZ (molecules per unit area); α is the excluded area per MZ molecule; β is a parameter, accounting for the interaction between the adsorbed molecules; K is an adsorption constant. [If we substitute eq 8.3 into the Gibbs adsorption equation, $d\sigma = -\Gamma kT\, d(\ln c_{MZ})$, and integrate, we derive eq 8.4.] Equations 8.3 and 8.4 give the theoretical dependence $\sigma(c_{MZ})$ in the following parametric form: $c_{MZ} = c_{MZ}(\Gamma)$ and $\sigma = \sigma(\Gamma)$.

The adsorption constant can be presented in the form $K = \alpha\delta \exp(E/kT)$ (see, e.g., eq 5 in ref 27). Here, δ is the length of the MZ molecule and, by definition, E is its adsorption energy in a standard state, in which the surfactant hydrocarbon tail is stretched and oriented normal to the interface. In view of eq 3.2 and the expression for K, the left-hand side of eq 8.4 can be presented in the form

$$Kc_{MZ} = \frac{c_M c_t \gamma_\pm^{\,2}}{Q_{MZ}} \alpha\delta \exp(E/kT) \tag{8.5}$$

$\gamma_\pm$ is given by eq 3.4. One could expect that the values of δ and E are not so different for HZ and MZ. For this reason (to decrease the number of adjustable parameters), for MZ we used the values δ = 2.215 nm and $E = 14.588kT$, calculated from eqs 6, 7, and 11 in ref 27 for myristic acid (n = 14), viz.,

$$\delta(n) = (0.154 + 0.1265n + 0.29)\ [\text{nm}]$$

$$E(n) = E_0 + 1.025nkT$$

where $1.025(\pm 0.020)kT$ (=604.5 cal/mol) is the energy for transfer of one CH_2 group from the water into the air,[43] and $E_0 = 0.2381kT$ (=140.4 cal/mol) accounts for the edge effects.[27]

The data for σ vs $X \equiv c_M c_t \gamma_\pm^2$ (Figure 18) were fitted by using eqs 8.3−8.5, which contain three adjustable parameters: α, β, and Q_{MZ}. We employed the least-squares method, and numerically minimized the function

$$\Phi(\alpha,\beta,Q_{MZ}) = \sum_{i=1}^{N}[\sigma_i - \sigma_{th}(X_i;\alpha,\beta,Q_{MZ})]^2 \qquad (8.6)$$

where N is the number of experimental points (X_i,σ_i), $i = 1, ..., N$, whereas σ_{th} is the theoretical value of the surface tension, calculated from eqs 8.3−8.5 for the same X_i.

It turns out that $\Phi(\alpha,\beta,Q_{MZ})$ has a sharp minimum with respect to its three arguments, from where we determined their values, as follows:

$$\alpha = 32.6\ \text{Å}^2, \quad \hat{\beta} \equiv \frac{2\beta}{\alpha kT} = 2.68, \quad Q_{MZ} = 2.84 \qquad (8.7)$$

The standard deviation of the experimental points with respect to the theoretical curve in Figure 18 is $\Delta\sigma = 0.40$ mN/m. The solid lines in Figure 3 correspond to the same best fit.

In the conventional van der Waals model, α can be interpreted as the geometrical cross-sectional area of the adsorbed molecule.[43] The value $\alpha = 32.6$ Å^2 obtained for a nondissociated NaMy molecule is greater than the value $\alpha = 22.6$ Å^2 obtained for fatty acids,[27] but it is smaller than the "equatorial" cross-sectional area of the hydrated Na^+ ion, 40.7 Å^2. (According to ref 48, the radius of the latter ion is $r_i = 3.6$ Å, and then $\alpha = \pi r_i^2 = 40.7$ Å^2.) This result implies that the Na atom in the headgroup of an adsorbed NaMy molecule is less hydrated than the free Na^+ ion, as it could be expected.

The value of the dimensionless interaction parameter for NaMy, $\hat{\beta} = 2.68$, is close to $\hat{\beta} = 2.73$ obtained for sodium dodecyl sulfate (SDS),[43] both of them being markedly smaller than the value 6.75 ($=3^3/2^2$) that corresponds to the gas/liquid-expanded phase transition in the framework of the van der Waals model. As known, positive $\hat{\beta}$ indicates the presence of attraction between the adsorbed molecules, which is usually attributed to van der Waals forces between the surfactant hydrocarbon tails.[44]

We recall that the above value of the dissociation constant of NaMy, $Q_{MZ} = 2.84$ M, is obtained from the fit (Figure 18) as an adjustable parameter, assuming that the adsorption energy, E, for a nondissociated NaMy molecule is the same as for a molecule of myristic acid. This assumption seems reasonable, because the main energy change during surfactant adsorption is related to the transfer of the hydrocarbon tail out of the water phase. (MZ and HZ have identical tails and, moreover, the −COO− portions of their headgroups are also identical.) With the above value of Q_{MZ}, we calculated $c_{MZ} = c_M c_Z \gamma_\pm^2 / Q_{MZ}$, which is plotted along the upper horizontal axis in Figure 18; see eq 3.2. The right-hand-side end-point of the curve in Figure 4b corresponds to the solubility limit of NaMy, $c_{MZ} = S_{MZ}$. Using the value of K_{MZ} in Table 2, and $Q_{MZ} = 2.84$ M, we obtain $S_{MZ} = K_{MZ}/Q_{MZ} = 1.09 \times 10^{-5}$ M. In other words, the nondissociated sodium myristate exhibits a considerably greater solubility than the myristic acid, for which we have $S_{HZ} = 5.25 \times 10^{-7}$ M (see ref 4).

9. Summary and Conclusions

We present new experimental data for the dependence of the natural pH of NaL and NaMy solutions on the carboxylate concentration at fixed content of NaCl (Figure 1). We obtained also surface-tension isotherms of NaL and NaMy in the presence of NaCl and NaOH (Figures 2 and 3). All experiments were carried out at 25 °C.

The theory of pH of carboxylate soap solutions with precipitates[4] is generalized to account for the presence of inorganic electrolyte, base, and formation of acid soaps of arbitrary stoichiometry, $(HZ)_j(MZ)_n$, $j,n = 1, 2, 3, ...$, see section 3. Special attention is paid to the case of precipitation of two solid-phases, acid soap and neutral soap, see section 3.5. A method for identification of the different precipitates from experimental data for pH vs c_t was developed. It is based on the analysis of precipitation diagrams (Figures 4, 8, 10, and 12), which represent plots of characteristic functions defined in section 4.

The theoretical analysis of the experimental data for pH of NaL solutions reveals the existence of three concentration regions: (i) without precipitates; (ii) with lauric acid precipitate, and (iii) with 1:1 acid-soap precipitate (Figure 5). The surface-tension isotherm of the NaL is insensitive to the concentration of added NaCl; it exhibits a kink at the threshold concentration for appearance of lauric acid precipitate, and has a plateau at higher concentrations (Figure 6). This behavior indicates that the adsorption monolayer is composed mostly of the nonionic lauric acid (HZ) with a small admixture of laurate anions (Z^-); see Figure 7.

In addition, the theoretical analysis of the pH of NaMy solutions without added salt shows the existence of five different concentration regions: (i) without precipitates; (ii) with precipitate of myristic acid (HZ); (iii) with precipitate of 4:1 acid soap, $(HZ)_4(MZ)_1$; (iv) with precipitate of 1:1 acid soap, $(HZ)_1(MZ)_1$; and (v) with coexistence of 1:1 acid soap and neutral soap (MZ) solid phases; see Figure 9. The addition of 10 mM NaCl transforms the 4:1 acid soap into 3:2 acid soap and shifts the boundaries between the precipitation zones (compare Figures 9 and 11a). In the presence of 100 mM NaCl, one observes the formation of precipitates from 1:1 acid soap alone, and coexistence of 1:1 acid soap and neutral soap; see Figure 13. The kinks in the surface-tension isotherm of NaMy (Figure 11b) correspond to transitions between concentration regions with different precipitates.

The solubility products (constants) for different types of precipitates, K_{MZ}, K_{11}, K_{32}, and K_{41}, have been determined (Table 2). The modeling of $(HZ)_j(MZ)_n$ acid soaps as solid solutions of alkanoic acid and 1:1 acid soap leads to a theoretical expression for K_{jn} ($j \geq n$), eq 7.10, which agrees well with the experimental results (Figure 15).

The effect of added base on the precipitates in the NaMy solutions was investigated both theoretically and experimentally (sections 3 and 8). The kinks in the surface tension isotherms of NaMy + 10 mM NaOH (Figure 3) can be attributed to precipitation of neutral soap (MZ); see Table 4. Furthermore, our analysis reveals (section 8.2) that, at lower NaMy concentrations, the solutions with 10 mM NaOH contain nondissociated NaMy molecules, which behave as a nonionic surfactant that dominates the surface tension (Figure 18). From the surface tension isotherms, we estimated the dissociation constant of NaMy: $Q_{MZ} = 2.84$ M.

The developed approach could be further applied to analyze the type of precipitates in sodium and potassium alkanoates with other chain lengths (palmitates, stearates, etc.), and to investigate the effect of temperature on the precipitation in various soap solutions.

Acknowledgment. We gratefully acknowledge the support of Unilever Research & Development, Trumbull, Connecticut, for this study. The authors are thankful to Dr. K. Marinova who took part in a part of the experiments.

LA0625401